Complete analysis of the Landau-gauge three-gluon vertex from lattice QCD

F. Pinto-Gómez,[1,2] F. De Soto,[2] and J. Rodríguez-Quintero[1]

[1]*Departamento de Ciencias Integradas, Centro de Estudios Avanzados en Física, Matemátics y Computación, Facultad Ciencias Experimentales, Universidad de Huelva, Huelva 21071, Spain*

[2]*Departamento de Sistemas Físicos, Químicos y Naturales, Universidad Pablo de Olavide, 41013 Sevilla, Spain*

(Received 17 April 2024; accepted 7 June 2024; published 8 July 2024)

Several continuum and lattice investigations of the QCD three-gluon vertex have recently exposed its key properties, some intimately connected with the low-momentum behavior of the two-point gluon Green's function and especially relevant for the emergence of a mass scale in this latter, via the Schwinger mechanism. In the present study, we report on a lattice determination of the Landau-gauge, transversely projected three-gluon vertex, particularly scrutinizing an outstanding one of these properties, termed *planar degeneracy*, exploring its implications and capitalizing on it to gain further insight on the low-momentum running of both the three-gluon vertex and its associated strong coupling.

DOI: 10.1103/PhysRevD.110.014005

I. INTRODUCTION

The understanding of the origin of mass is one of the most challenging, still open questions in particle physics. The Higgs mechanism is well understood as responsible for the masses of electroweak interacting bosons and all leptons. However, concerning hadrons and especially those composing stable matter, it can explain only just 1%–2% of the nucleons' masses. The hadrons are composite bound states whose mass budget cannot be explained by the single contribution of their elementary components, the Lagrangian (current) quark masses, and mostly relies on the dynamics of quantum chromodynamics (QCD), the Standard Model's strong interaction theory [1–5]. The hadron masses basically *emerge* from the interactions of quarks and gluons [6], although the nature of the interacting gluons is very much determined by the gluon-gluon interaction, which is an expression of a key feature of QCD: its non-Abelian character. This same character triggers the antiscreening of color charges, which drives the interaction strength from its asymptotically free limit at low distances to a nonperturbative regime at low energies. And it is in this last that the rich and intriguing dynamics of QCD becomes apparent.

The way in which gluon self-interactions define gluon properties is revealed by a central component of QCD, the three-gluon vertex [7–9]. It has been established [10–16] that the presence of longitudinally coupled massless-pole structures in the three-gluon vertex activates the so-called Schwinger mechanism [17–22], generating thereby a dynamical gluon mass and rendering the two-point gluon Green's function finite at vanishing momentum. This latter fact and that the ghost is transparent to the mass generation mechanism have been confirmed by a variety of studies of the fundamental QCD Green's functions carried out in both continuum [23–46] and lattice QCD [47–50].

As the other side of the coin, when a dynamical gluon mass is generated, the interplay of massive gluon and massless ghost propagators, involved in the Dyson-Schwinger equations (DSE) expansions of QCD Green's functions, generates logarithmic singularities at the two- and three-point levels connected by the corresponding Slavnov-Taylor identities (STIs) [51,52]. The two-point singularity comes from the ghost-loop contribution to the gluon self-energy, tamed by a kinematic factor q^2 and appearing only as a maximum in the gluon propagator form factor at nonzero momentum. However, it remains dynamically attached by the mass generation mechanism to the three-point singularity, associated to the tree-level tensor structure of the three-gluon vertex, where it is manifest in its corresponding form factor by crossing zero at low momentum, after an infrared suppression caused by the contributions from the usually called *swordfish* diagrams [53]. These properties for the three-gluon vertex have been unveiled by a series of recent works [51–74] and have been revealed as instrumental for the formation of physically meaningful bound states [75–83].

Particularly in lattice QCD, the vertex form factors of two special classes of kinematic configurations, *soft-gluon* and *symmetric*, in which the vertex tensor space becomes reduced, have been extensively studied with both quenched

[64–67] and unquenched [57] simulations in Landau gauge. Only very recently, a more general analysis extended to all available triplets of momenta with two equal squared ones, dubbed *bisectoral* configurations, has been performed [73,74]. As a main outcome of this analysis, a three-gluon vertex property, termed therein *planar degeneracy* and anticipated in some aspects by a previous DSE study [59], is established. This property tells that, in very good approximation over a wide momentum range, the significant form factor is the one associated to the tree-level (classical) tensor and its behavior is driven by only one Bose-symmetric combination of the three squared momenta. A first important consequence of this was soon exposed by a subsequent study [16], in which a three-gluon vertex constructed with lattice QCD inputs by assuming planar degeneracy has been used to evaluate deviations in its corresponding STIs, shown to be consistent with the longitudinally coupled massless poles triggering the Schwinger mechanism for the generation of a dynamical gluon mass.

In the current work, for the first time, we extend the study of the three-gluon vertex obtained from lattice QCD in Landau gauge to a fully general kinematics, beyond the bisectoral class, furthermore implementing a complete, improved tensor basis [53]. We will initially focus on a proper analysis of lattice discretization artifacts and, next, scrutinize the deviations from planar degeneracy, paying special attention to the behavior of the nonclassical form factors and their impact. Then, we will canvass the implications of this remarkable property and, capitalizing on it, elaborate further on the description of the non-perturbative running of the three-gluon vertex. An outstanding inference from planar degeneracy is its entailing a unique definition for the renormalized three-gluon vertex [viz. Eq. (40)] and effective coupling [viz. Eq. (42)], provided that the subtraction point is rationally defined. Furthermore, capitalizing on previous investigations of the soft-gluon and symmetric kinematic configurations from lattice QCD with $2+1$ dynamical fermions simulated with a domain-wall action (DWF) [70], we deliver the first unquenched results based on planar degeneracy.

II. THE THREE-GLUON VERTEX

The starting step in our computational scheme is the calculation of the three-point correlation function in Fourier space $\langle \tilde{A}^a_\alpha(q)\tilde{A}^b_\mu(r)\tilde{A}^c_\nu(p)\rangle$, where $\tilde{A}^a_\alpha(q)$ corresponds to the gauge-field Lorentz-color component $\{\alpha, a\}$ at four-momentum q and $\langle\cdots\rangle$ stands for the average over the Landau-gauge field configurations. More particularly, we will focus on its projection over the antisymmetric color tensor f^{abc}:

$$\mathcal{G}_{\alpha\mu\nu}(q,r,p) = \frac{1}{24} f^{abc}\langle \tilde{A}^a_\alpha(q)\tilde{A}^b_\mu(r)\tilde{A}^c_\nu(p)\rangle, \qquad (1)$$

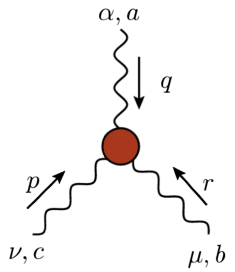

FIG. 1. Diagrammatic representation of the 1PI three-gluon vertex with the prescription chosen for the momenta and Lorentz-color indices.

thereby discarding any possible contribution in the symmetric color tensor d^{abc}.

The three-gluon vertex depends on three momenta kinematically constrained by momentum conservation, $q+r+p=0$, which allows that any possible tensor should be formed by their different combinations, also including the metric tensor: e.g., $q_\alpha q_\mu q_\nu$ or $g_{\alpha\mu}p_\nu$. In total, there are 14 linearly independent tensors [8,84], although only four survive in Landau gauge owing to the transverse condition $q_\alpha\mathcal{G}_{\alpha\mu\nu}(q,r,p) = r_\mu\mathcal{G}_{\alpha\mu\nu}(q,r,p) = p_\nu\mathcal{G}_{\alpha\mu\nu}(q,r,p) = 0$.

As discussed at length in Refs. [64–66], one can define the transverse projection of the one-particle irreducible (1PI) three-gluon vertex $\mathrm{I\Gamma}^{\alpha'\mu'\nu'}$ (sketched in Fig. 1):

$$\bar{\Gamma}_{\alpha\mu\nu}(q,r,p) = \mathrm{I\Gamma}^{\alpha'\mu'\nu'}(q,r,p)P_{\alpha'\alpha}(q)P_{\mu'\mu}(r)P_{\nu'\nu}(p), \qquad (2)$$

with $P_{\mu\nu}(q) = g_{\mu\nu} - q_\mu q_\nu/q^2$ standing for the usual transverse projector; which can be thus derived from $\mathcal{G}_{\alpha\mu\nu}(q,r,p)$ as

$$g\bar{\Gamma}_{\alpha\mu\nu}(q,r,p) = \frac{\mathcal{G}_{\alpha\mu\nu}(q,r,p)}{\Delta(q^2)\Delta(r^2)\Delta(p^2)}, \qquad (3)$$

where g is the strong coupling and $\Delta(q^2)$ is defined from the gluon propagator as

$$\langle \tilde{A}^a_\mu(q)\tilde{A}^b_\mu(-q)\rangle = \delta^{ab}P_{\mu\nu}(q)\Delta(q^2). \qquad (4)$$

This *transversely projected vertex* $\bar{\Gamma}_{\alpha\mu\nu}$ is the quantity that can be estimated from Landau-gauge lattice QCD simulations, from which the three-point correlation function in Eq. (1) can be calculated. It can be highlighted that it receives no contribution from the longitudinally coupled massless poles [11–13] shown to trigger the Schwinger mechanism [16–22]. This transverse projection of the pole-free component of the 1PI three-gluon vertex is the object we will deal with in what follows.

A. Bose-symmetric basis

Embedded only within the 4D transverse subspace of the tensor space defined by the 1PI three-gluon vertex, $\bar{\Gamma}_{\alpha\mu\nu}$ can

be generally written in terms of any basis made by four linearly independent transverse tensors. Particularly, the choice of basis tensors expressing explicitly the Bose symmetry of the three-point Green function from Eq. (1) is advantageous, as has been detailed in Ref. [73] and will be again exploited below. A simple inspection of Eq. (1) makes apparent that, as f^{abc} is antisymmetric under exchange of color indices, so are, too, $\mathcal{G}_{\alpha\mu\nu}(q,r,p)$, and, hence, $\bar{\Gamma}_{\alpha\mu\nu}(q,r,p)$ defined by Eq. (3), under the simultaneous exchange of two momenta and their corresponding Lorentz indices. Then, one is left with [73]

$$\bar{\Gamma}_{\alpha\mu\nu}(q,r,p)=\sum_{i=1}^{4}\tilde{\Gamma}_i(q^2,r^2,p^2)\tilde{\lambda}_{i\alpha\mu\nu}(q,r,p), \quad (5)$$

with

$$\tilde{\lambda}_{1\alpha\mu\nu}(q,r,p)=[\ell_1^{\alpha'\mu'\nu'}+\ell_4^{\alpha'\mu'\nu'}+\ell_7^{\alpha'\mu'\nu'}]P^{\alpha}_{\alpha'}(q)P^{\mu'}_{\mu}(r)P^{\nu'}_{\nu}(p), \quad (6a)$$

$$\tilde{\lambda}_{2\alpha\mu\nu}(q,r,p)=3\frac{(q-r)_{\nu'}(r-p)_{\alpha'}(p-q)_{\mu'}}{q^2+r^2+p^2}\times P^{\alpha'}_{\alpha}(q)P^{\mu'}_{\mu}(r)P^{\nu'}_{\nu}(p), \quad (6b)$$

$$\tilde{\lambda}_{3\alpha\mu\nu}(q,r,p)=\frac{3}{q^2+r^2+p^2}\left[\ell_3^{\alpha'\mu'\nu'}+\ell_6^{\alpha'\mu'\nu'}+\ell_9^{\alpha'\mu'\nu'}\right]\times P^{\alpha}_{\alpha'}(q)P^{\mu}_{\mu'}(r)P^{\nu}_{\nu'}(p), \quad (6c)$$

$$\tilde{\lambda}_{4\alpha\mu\nu}(q,r,p)=\left(\frac{3}{q^2+r^2+p^2}\right)^2\left[t_1^{\alpha\mu\nu}+t_2^{\alpha\mu\nu}+t_3^{\alpha\mu\nu}\right], \quad (6d)$$

where t_i and l_j stand, respectively, for the four transverse and ten nontransverse, well-known Ball-Chiu tensors [8,84] [see, e.g., Eqs. (3.4) and (3.6) in Ref. [52]]. The basis tensors given by Eq. (6) can be proven to express the antisymmetric character of $\bar{\Gamma}_{\alpha\mu\nu}(q,r,p)$ under Bose transformations: e.g., $\tilde{\lambda}_{i\alpha\mu\nu}(q,r,p)=-\tilde{\lambda}_{i\mu\alpha\nu}(r,q,p)$. However, keeping this antisymmetric property, other choices are possible and, in some aspects, preferable.

Let us generally consider another tensor basis such that

$$\bar{\Gamma}_{\alpha\mu\nu}(q,r,p)=\sum_{i=1}^{4}\tilde{\Gamma}^*_i(q^2,r^2,p^2)\tilde{\lambda}^*_{i\alpha\mu\nu}(q,r,p), \quad (7)$$

where one and another form factors can be related as

$$\tilde{\Gamma}^*_i(q^2,r^2,p^2)=\mathcal{P}^{*\alpha\mu\nu}_i\bar{\Gamma}_{\alpha\mu\nu}(q^2,r^2,p^2) \quad (8a)$$

$$=\sum_{k=1}^{4}\mathcal{P}^{*\alpha\mu\nu}_i\tilde{\lambda}_{k\alpha\mu\nu}(q,r,p)\tilde{\Gamma}_k(q^2,r^2,p^2), \quad (8b)$$

where Eq. (8a) displays the form factors projected out from $\bar{\Gamma}_{\alpha\mu\nu}(q,r,p)$, as it is expanded in (7), with the projector

$$\mathcal{P}^{*\alpha\mu\nu}_i=\sum_{j}^{4}\tilde{M}^{*-1}_{ij}(q^2,r^2,p^2)\tilde{\lambda}^{*\alpha\mu\nu}_j(q,r,p), \quad (9)$$

defined by the 4×4 matrix

$$\tilde{M}^*_{ij}(q^2,r^2,p^2)=\tilde{\lambda}^{*\alpha\mu\nu}_i(q,r,p)\tilde{\lambda}^*_{j\alpha\mu\nu}(q,r,p); \quad (10)$$

while (8b) results from replacing the vertex with its expansion given by Eq. (5).

The basis defined by Eq. (6) has been introduced in Ref. [73] as a generalization of the restricted one employed in Refs. [64–66]. Indeed, $\tilde{\lambda}_{1\alpha\mu\nu}(q,r,p)$ corresponds to the three-gluon tree-level tensor which, together with $\tilde{\lambda}_{2\alpha\mu\nu}(q,r,p)$, forms a basis for those special kinematic configurations in which the three squared momenta are equal (*symmetric* case); while $\tilde{\lambda}_{3\alpha\mu\nu}(q,r,p)$ and $\tilde{\lambda}_{4\alpha\mu\nu}(q,r,p)$ were therein chosen for the basis completion in the 4D transverse subspace. An alternative choice [53] can be featured as

$$\tilde{\lambda}^*_{i\alpha\mu\nu}(q,r,p)=\tilde{\lambda}_{i\alpha\mu\nu}(q,r,p)-\delta_{i3}\frac{3}{2}\tilde{\lambda}_{1\alpha\mu\nu}(q,r,p), \quad (11)$$

implying that Eq. (8b) specializes as

$$\tilde{\Gamma}^*_i(q^2,r^2,p^2)=\sum_{k=1}^{4}\left(\delta_{ik}+\frac{3}{2}\delta_{i1}\delta_{k3}\right)\tilde{\Gamma}_k(q^2,r^2,p^2). \quad (12)$$

The latter will be shown below as a very useful result entailing that, after the redefinition of the basis by Eq. (11), the form factor $\tilde{\Gamma}^*_1(q^2,q^2,0)$ fully delivers the soft-gluon limit ($p^2\to 0$) of the transversely projected vertex [53].

B. Kinematics

Owing to momentum conservation, a kinematic configuration for the three-gluon vertex remains entirely determined by the three squared momenta or, alternatively, by two momenta and the angle they form (e.g., q^2, r^2 and $\theta_{qr}=[p^2-q^2-r^2]/[2\sqrt{q^2r^2}]$, or any completely analogous combination). Furthermore, the scalar form factors defined in Eqs. (5) and (7), which depend on three scalars, can be equivalently characterized. Interestingly, the basis being Bose-symmetric, they can depend only on Bose invariants that can be recast as[1]

[1]For reference, it is convenient to write these invariants in terms of the ones defined in Eqs. (50) and (53) in [59], $\mathcal{S}_0$, $\mathcal{S}_1$, and $\mathcal{S}_2$: $s^2=3\mathcal{S}_0$, $t^4=6\mathcal{S}_0^2\mathcal{S}_1$, and $u^6=54\mathcal{S}_0^3\mathcal{S}_2$.

$$s^2 = \frac{q^2 + r^2 + p^2}{2}, \tag{13a}$$

$$t^4 = \frac{(q^2 - r^2)^2 + (r^2 - p^2)^2 + (p^2 - q^2)^2}{3}, \tag{13b}$$

$$u^6 = (q^2 + r^2 - 2p^2)(r^2 + p^2 - 2q^2)(p^2 + q^2 - 2r^2). \tag{13c}$$

An extensive analysis of the three-gluon kinematic configurations is done in Ref. [59] on the ground of the theory of permutation group; while a geometric rederivation can be found in Ref. [73]. In the aim of keeping enough self-completion in the present document, we will shortly outline their main outcomes.

Any possible kinematical configuration, characterized by the three squared momenta, can be represented as a point in the positive octant of a 3D space, whose Cartesian axes correspond to q^2, r^2 and p^2 (see the top-right plot in Fig. 2). All configurations sharing the same s invariant, Eq. (13a), sit on a plane perpendicular to the diagonal of this positive octant (the distance of the plane to the origin along the diagonal is $2s^2/\sqrt{3}$), which defines an equilateral triangle (drawn in blue in the figure). Furthermore, momentum conservation, $q + r + p = 0$, imposes a restriction on the momenta such that all allowed configurations lie within the triangle incircle, the center of which corresponds to the symmetric configuration: $q^2 = r^2 = p^2$ (represented by a green dot). The t invariant, Eq. (13b), locates the point representing the configuration on a given concentric circumference within the incircle and expresses its separation away from the symmetric case (momentum conservation translates into $t^2 \leq \sqrt{2/3}s^2$). And, finally, the u invariant, Eq. (13c), refers to the location to each of the three bisectoral lines in the triangle. As discussed in Ref. [73], all the configurations such that two squared momenta and two angles are the same can be represented by a piece of bisectoral line lying inside the incircle (e.g., the vertical one in Fig. 2 corresponds to $r^2 = q^2$ and $\theta_{qp} = \theta_{rp}$). Along any of the three bisectoral segments, the kinematics evolves from soft-gluon to collinear nonsoft cases, with the symmetric one in between; e.g., from the cases $p = 0$ and $\theta_{qp} = \theta_{rp} = \pi/2$ (orange point) to $q^2 = r^2 = p^2/4$ and $\theta_{qp} = \theta_{rp} = \pi$ (in Landau gauge, no tensor structure remains for this case), passing through $q^2 = p^2 = r^2$ and $\theta_{pq} = \theta_{rp} = 2\pi/3$ (green point), as illustrated in the vertical bisectoral in Fig. 2. And, accordingly, the u invariant evolves from $u^6 = 2s^6$ (soft-gluon) to $u^6 = -2s^6$ (collinear nonsoft), becoming zero in the symmetric case.

It is worthwhile to underline that the incircle representing all allowed configurations can be divided into three identical regions, covering each an angle $2\pi/3$, that can be mapped into each other by permutations of the squared momenta q^2, r^2, and p^2, which do not modify the Bose-symmetric invariants defined in Eq. (13). In Fig. 2, these

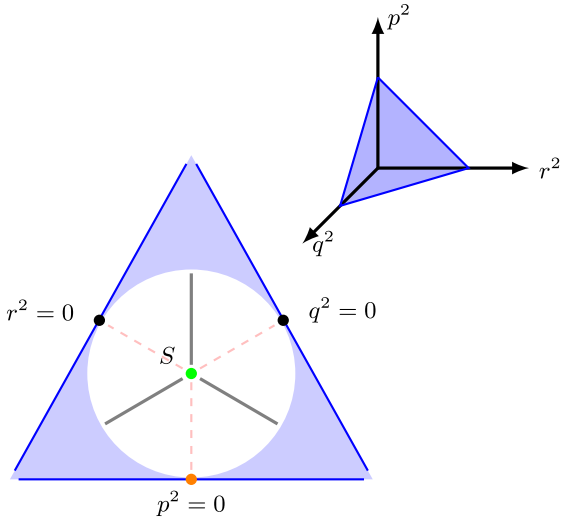

FIG. 2. The kinematic configurations for the three-gluon vertex sketched in Fig. 1, represented here by the Cartesian coordinates (q^2, r^2, p^2). A fixed value of s^2, Eq. (13a), implies sitting on the same plane perpendicular to the octant diagonal (top right), which defines an equilateral triangle in which momentum conservation restricts the representations to lie within the white incircle (left). The green dot labels the symmetric case, while black and orange stand for the soft-gluon, the latter specializing the case considered, and connected by permutations with the other two. The explanation of this representation is expanded in the text.

three regions appear bordered by solid gray lines displaying the bisectoral segments which join the symmetric and collinear nonsoft cases. On top of this, Bose symmetry[2] also guarantees that the invariants remain unmodified by the reflection in respect to the bisectoral segment joining symmetric and soft-gluon cases, drawn with a pink dashed line in the figure. Therefore, only the kinematic configurations represented by points within one of the six regions delimited by solid gray and dashed pink lines, spanned by an angle $\pi/3$, are independent.

In general, the transversely projected vertex can have independent contributions in the four basis tensors defined by either Eq. (6) or (11), with the corresponding form factors projected out by applying Eq. (8a) and, in the former case, also Eq. (12). They may depend on the three invariants (13) that can be evaluated for any arbitrary kinematic configuration.

However, we will begin by specializing for the bisectoral kinematics, as in Ref. [73], highlighting the particular soft-gluon and symmetric cases. With no loss of generality, one can then focus on the case $q^2 = r^2$ and $\theta_{pq} = \theta_{pr}$, for any p^2. The subspace spanned by the transversely projected vertex reduces thereby its dimension from 4 down to 3, and

[2]The operation of reflection in respect to the bisectoral segment joining the symmetric and the $p = 0$ case corresponds to the exchange $q^2 \leftrightarrow r^2$; completely analogous properties hold for the other two bisectoral segments.

the new restricted tensor basis obtained from Eq. (11) is formed by the three tensors

$$\bar{\lambda}^*_{i\alpha\mu\nu}(q,r,p) = \lim_{r^2\to q^2} \tilde{\lambda}^*_{i\alpha\mu\nu}(q,r,p), \tag{14}$$

for $i = 1, 2, 3$; while

$$\lim_{r^2\to p^2} \tilde{\lambda}^*_{4\alpha\mu\nu}(q,r,p) = \sum_{i=1}^{3} f^*_i\left(\frac{2p^2}{p^2+2q^2}\right)\tilde{\lambda}^*_{i\alpha\mu\nu}(q,r,p), \tag{15}$$

with

$$f^*_1(z) = \frac{9}{16}z(2-z), \quad f^*_2(z) = \frac{3}{8}\left(\frac{3}{4}z-1\right), \quad f^*_3(z) = \frac{3}{8}z. \tag{16}$$

A restricted basis of tensors $\bar{\lambda}_{i\alpha\mu\nu}$ can be analogously derived from (6) and formally identical results obtained with the only difference that $f_1(z) = 9/16z(1-z)$ [73].

Then, Eqs. (8)–(10) can be specialized to the bisectoral case only with the replacement of 4D by 3D basis tensors, restricting the running of i, j, and k from 1 to 3. This entails for the noninvertible 4×4 matrix (10) its being replaced by its first 3×3 block in the limit $r^2 \to q^2$:

$$\bar{M}^*_{ij}(q^2,p^2) = \lim_{r^2\to q^2} \tilde{M}^*_{ij}(q^2,r^2,p^2) \tag{17}$$

for $i, j = 1, 2, 3$; the form factors for the restricted basis reading now

$$\bar{\Gamma}^*_i(q^2,p^2) = \lim_{r^2\to q^2} \tilde{\Gamma}^*_i(q^2,r^2,p^2) + f^*_i\left(\frac{2p^2}{p^2+2q^2}\right)\tilde{\Gamma}^*_4(q^2,r^2,p^2), \tag{18}$$

in terms of those for the general basis. And a formally identical equation holds relating the form factors $\tilde{\Gamma}_i$'s and $\bar{\Gamma}_i$'s defined from Eqs. (5) and (6). Analogously, in the bisectoral case, an equation equivalent to (12) works to make $\bar{\Gamma}^*_i$'s read in terms of $\bar{\Gamma}_k$'s, with $i, k = 1, 2, 3$.

The symmetric ($p^2 = q^2 = r^2$, $\theta_{pq} = \theta_{pr} = 2\pi/3$) and soft-gluon ($p^2 = 0$, $\theta_{pq} = \theta_{pr} = \pi/2$) are special cases in which the 3×3 matrix defined in Eq. (17) is noninvertible, as the involved tensor subspaces take dimensions 2 and 1, respectively, making its determinant vanish.

In the symmetric case, the new restricted basis can be defined as [$i = 1, 2$]

$$\lambda_{i\alpha\mu\nu}(q,r,p) = \lim_{p^2\to q^2} \bar{\lambda}_{i\alpha\mu\nu}(q,r,p) = \lim_{p^2\to q^2} \bar{\lambda}^*_{i\alpha\mu\nu}(q,r,p), \tag{19}$$

in terms of which, the transversely projected vertex reads

$$\bar{\Gamma}_{\alpha\mu\nu}(r,q,p) = \sum_{i=1}^{2} \bar{\Gamma}^{\rm sym}_i(q^2)\lambda_{i\alpha\mu\nu}(q,r,p), \tag{20}$$

with

$$\bar{\Gamma}^{\rm sym}_1(q^2) = \lim_{p^2\to q^2} \bar{\Gamma}_1(q^2,p^2) + \frac{1}{2}\bar{\Gamma}_3(q^2,p^2) \tag{21a}$$

$$\lim_{p^2\to q^2} \bar{\Gamma}^*_1(q^2,p^2) - \bar{\Gamma}^*_3(q^2,p^2), \tag{21b}$$

$$\bar{\Gamma}^{\rm sym}_2(q^2) = \lim_{p^2\to q^2} \bar{\Gamma}_2(q^2,p^2) - \frac{3}{4}\bar{\Gamma}_3(q^2,p^2) \tag{21c}$$

$$= \lim_{p^2\to q^2} \bar{\Gamma}^*_2(q^2,p^2) - \frac{3}{4}\bar{\Gamma}^*_3(q^2,p^2). \tag{21d}$$

On the other hand, in the soft-gluon case, one is left only with the tree-level tensor $\lambda_{1\alpha\mu\nu}(q,r,p)$, which corresponds to $\bar{\lambda}^*_{1\alpha\mu\nu}(r,q,p) = \bar{\lambda}_{1\alpha\mu\nu}(r,q,p)$ taken in the limit $p \to 0$, and can, thus, write

$$\bar{\Gamma}_{\alpha\mu\nu}(r,q,p) = \bar{\Gamma}^{\rm sg}(q^2)\lambda_{1\alpha\mu\nu}(q,r,p), \tag{22}$$

with

$$\bar{\Gamma}^{\rm sg}(q^2) = \lim_{p^2\to 0} \bar{\Gamma}_1(q^2,p^2) + \frac{3}{2}\bar{\Gamma}_3(q^2,p^2) \tag{23a}$$

$$= \lim_{p^2\to 0} \bar{\Gamma}^*_1(q^2,p^2). \tag{23b}$$

The outcome exhibited by Eq. (23), which can be traced back to Eq. (12), appears as the main advantage of the tensor basis (11), Ref. [53], in respect to (6), Ref. [73]. Namely, the unique form factor in the soft-gluon case is given only by the appropriate limit of the tree-level tensor form factor; while, is the basis (6) used, two form factors will need to be combined to deliver the correct result. As it is raised in Ref. [73], both $\bar{\Gamma}_1(q^2,p^2)$ and $\bar{\Gamma}_3(q^2,p^2)$ are separately plagued by a perturbative divergence in the limit $p \to 0$, which, however, cancels out when they are combined as in Eq. (23a), rendering finite and well defined the soft-gluon form factor and, owing to (23b), the bisectoral $\bar{\Gamma}^*_1(q^2,p^2)$. These divergences in $\bar{\Gamma}_{1,2}(q^2,p^2)$ have been seen to be individually tamed by the nonperturbative generation of a gluon mass [16,53]. However, as will be discussed below, their remnant seems to spoil in some kinematic region some of the good properties of the three-gluon form factors, making especially useful their being removed by the implementation of the tensor basis (11).

C. Renormalization of the three-gluon form-factors and coupling

We have thus far elaborated on the derivation of the relevant form factors for the transversely projected vertex $\bar{\Gamma}_{\alpha\mu\nu}$ from the three-point Green's function $\mathcal{G}_{\alpha\mu\nu}$. The latter is herein computed from lattice QCD and, thereby, obtained as a lattice-regularized bare quantity. A multiplicative renormalization scheme is subsequently applied by introducing first the gauge-field renormalization constant Z_A, such that bare and renormalized gluon two- and three-point Green functions relate as

$$\Delta_R(q^2) = \lim_{a\to 0} Z_A^{-1}(a)\Delta(q^2;a), \tag{24a}$$

$$\mathcal{G}_{R\alpha\mu\nu}(q,r,p) = \lim_{a\to 0} Z_A^{-3/2}(a)\mathcal{G}_{\alpha\mu\nu}(q,r,p;a), \tag{24b}$$

where we have made explicit the dependence on the regularization scale, the lattice spacing a, of the bare quantities and renormalization constants and have left implicit the latter's and renormalized quantities' on the subtraction scale ζ^2. Capitalizing on multiplicative renormalizability, only one further renormalization constant needs to be introduced for all the form factors of the 1PI three-gluon vertex:

$$\tilde{\Gamma}^*_{iR}(q^2,r^2,p^2) = \lim_{a\to 0} Z_3(a)\tilde{\Gamma}^*_i(q^2,r^2,p^2;a), \tag{25}$$

thus implying

$$g_R = \lim_{a\to 0} Z_A^{3/2}(a) Z_3^{-1}(a) g(a) \tag{26}$$

for the renormalization of the strong coupling. The same reads for the form factors from Eq. (5) for the tensor basis (6).

The last step of the calculation program is the implementation of a renormalization prescription, namely, *momentum subtraction* (MOM) [85] in our case. This implies that all renormalized correlation functions acquire their tree-level expressions at the subtraction point, defined in terms of the subtraction scale ζ^2. In particular, one sets $\Delta_R^{-1}(\zeta^2) = \zeta^2$, which fixes Z_A:

$$Z_A(a^2) = \zeta^2\Delta(\zeta^2;a); \tag{27}$$

while, for the three-gluon Green's function, one needs to consider a given kinematic configuration, Z_3 resulting defined by

$$\tilde{\Gamma}^*_{1R\mathrm{k}(\zeta)}(q^2,r^2,p^2)\big|_{\mathrm{k}(\zeta)} = \lim_{a\to 0} Z_3^{\mathrm{k}(\zeta)}(a)\tilde{\Gamma}^*_1(q^2,r^2,p^2;a)\big|_{\mathrm{k}(\zeta)} = 1, \tag{28}$$

where $\mathrm{k}(\zeta) \equiv \{\zeta^2, \theta_{qp}, \theta_{rp}\}$ specifies the chosen configuration and $R\mathrm{k}(\zeta)$ its associated renormalization scheme. At this point, we take advantage of the three-gluon kinematic analysis described in the previous subsection and choose a configuration represented by a point lying on the plane $s^2 = \zeta^2$, within the white circle in Fig. 2, fixed by two angles θ_{qp} and θ_{rp}.

In Eqs. (24)–(26) and (28), the limit $a \to 0$, required to drop any subleading lattice artifact away, has been made explicit. This is a mandatory part of a renormalization program, intended to remove properly any remaining nonsingular dependence on the regularization scale or cutoff, after subtraction. In lattice QCD calculations, the latter entails an extrapolation to the continuum limit which for the gluon and ghost propagators can be done by following the procedure detailed in [86]. However, when three-point functions are involved, the subleading lattice artifacts, once those related to $O(4)$ breaking are properly treated (as will be discussed below), become hidden by the statistical errors and, even at nonzero but small lattice spacing, the renormalized quantities appear not to depend on it. The limit $a \to 0$ can be then removed in practice, but, formally at least, Eq. (27) and

$$Z_3^{\mathrm{k}(\zeta)}(a) = (\tilde{\Gamma}^*_1(q^2,r^2,p^2;a)\big|_{\mathrm{k}(\zeta)})^{-1} \tag{29}$$

are only possible solutions, all differing only by subleading $\mathcal{O}(a^2)$ artifacts, of (24a) evaluated at $q^2 = \zeta^2$ and Eq. (28), respectively. They imply

$$\tilde{\Gamma}^*_{iR\mathrm{k}(\zeta)}(q^2,r^2,p^2) = \lim_{a\to 0} \frac{\tilde{\Gamma}^*_i(q^2,r^2,p^2;a)}{\tilde{\Gamma}^*_1(q^2,r^2,p^2;a)\big|_{\mathrm{k}(\zeta)}}, \tag{30}$$

for $i = 1,\ldots,4$, and

$$g_{R\mathrm{k}}(\zeta^2) = \lim_{a\to 0} \zeta^3\Delta^{3/2}(\zeta^2;a)\tilde{\Gamma}^*_1(q^2,r^2,p^2;a)\big|_{\mathrm{k}(\zeta)} g(a), \tag{31}$$

for the strong coupling, which is shown here with its explicit dependence on the subtraction scale.

We will make, for the three-gluon vertex renormalization, the same choice made in Ref. [73], that is, the so-called soft-gluon MOM scheme,[3] namely, $\mathrm{k}(\zeta) = \mathrm{s}(\zeta) \equiv \{\zeta^2, \pi/2, \pi/2\}$. Alternatively, another natural choice for the kinematic configuration at the subtraction point might have been the symmetric one: $\mathrm{k}(\zeta) = \mathrm{y}(\zeta) \equiv \{\zeta^2, 2\pi/3, 2\pi/3\}$; i.e.,

[3]Indeed, the soft-gluon kinematic configuration ($p^2 = 0$, $r^2 = q^2$) seems to be affected by an apparent ambiguity when is defined in terms of angles, as the condition appears to be $\theta_{rp} + \theta_{qp} = \pi$, for whichever θ_{rp} and θ_{qp}. Such an ambiguity can be seen not to exist, as, after a careful analysis [66,67], no trace of an individual dependence on the angles remains in the limit $\theta_{pq} + \theta_{rp} \to \pi$.

$$Z_3^{\mathrm{y}(\zeta)}(a) = \left(\tilde{\Gamma}_1^*\left(\frac{2}{3}\zeta^2, \frac{2}{3}\zeta^2, \frac{2}{3}\zeta^2; a\right)\right)^{-1}. \quad (32)$$

However, early applications of the MOM prescription for computing the renormalized coupling [87–90], as well as more recent analyses [57,91,92], have used instead a slightly different definition of the symmetric MOM scheme: $\bar{\mathrm{y}}(\zeta) \equiv \{3/2\zeta^2, 2\pi/3, 2\pi/3\}$, such that

$$Z_3^{\bar{\mathrm{y}}(\zeta)}(a) = (\tilde{\Gamma}_1^*(\zeta^2, \zeta^2, \zeta^2; a))^{-1}. \quad (33)$$

Both Eqs. (32) and (33) corresponding to symmetric configurations for the subtraction point, they basically differ by the choice of the invariant s^2 and are consequently represented by points lying on different planes in Fig. 2.

However, all renormalized form factors can be straightforwardly related to any other on the ground of Eqs. (29) and (30). While, for the strong coupling, one can derive from Eq. (31) that

$$g_{R\mathrm{k}}(\zeta^2) = \frac{\tilde{\Gamma}_1^*(q^2, r^2, p^2; a)|_{\mathrm{k}(\zeta)}}{\tilde{\Gamma}^{\mathrm{sg}}(\zeta^2; a)} g_{R\mathrm{s}}(\zeta^2) \quad (34a)$$

$$= \tilde{\Gamma}^*_{1\,R\mathrm{s}(\zeta)}(q^2, r^2, p^2)|_{\mathrm{k}(\zeta)} g_{R\mathrm{s}}(\zeta^2), \quad (34b)$$

relating three-gluon couplings in any MOM renormalization scheme Rk [with the subtraction point fixed at $k(\zeta)$] to Rs [at $s(\zeta)$; soft-gluon] through the ratio of their bare tree-level form factors or, alternatively, the renormalized form factor which comes out from that ratio.

III. RESULTS

As explained in Sec. II A, we can apply the projector defined by Eq. (9) to extract the form factors $\tilde{\Gamma}_i^*$ or, equivalently, its analog associated to the tensor basis (6) for $\tilde{\Gamma}_i$, from the transversely projected vertex calculated with lattice QCD bare Green's functions as shown in Eq. (3). In Refs. [73,74], we have already presented a first careful analysis of the three-gluon form factors $\bar{\Gamma}_i$ in bisectoral kinematics from lattice QCD. A main outcome of that analysis appeared to be the emergence of a property for these form factors, very specially for the tree-level one, named therein *planar degeneracy*, that can be simply described as their keeping dependence, in very good approximation, only on the s invariant, Eq. (13a).

Assumed beyond the bisectoral kinematics, as suggested therein[4] and applied next to confirm the Schwinger mechanism in Ref. [16], planar degeneracy implies that

TABLE I. Lattice setups for the gauge-field configurations used in this paper. The lattice spacings in the third column have been obtained using the absolute calibration reported in [93] at $\beta = 5.8$ and supplemented by a relative calibration based in the gluon propagator scaling following the procedure described in [86].

β	$(L/a)^4$	a (fm)	Configurations
5.6	32	0.236	2000
5.7	32	0.182	1000
5.8	32	0.144	2000
6.0	32	0.096	2000
6.2	32	0.070	2000
6.4	32	0.054	1290

$$\tilde{\Gamma}^*_{1\,R\mathrm{s}(\zeta)}(q^2, r^2, p^2)|_{\mathrm{k}(\zeta)} = 1, \quad (35)$$

as far as evaluation at $\mathrm{k}(\zeta)$ kinematics indicates that $s^2 = \zeta^2$, for any values of θ_{pq} and θ_{pr}; and the scheme $R\mathrm{s}(\zeta)$ fixes the subtraction point at $s^2 = \zeta^2$ with $\theta_{pq} = \theta_{pr} = \pi/2$. In short, required to take the value of 1 by the renormalization condition at the subtraction point, the renormalized tree-level form factor takes the same value for all angles because it keeps only dependence on s^2 (this result is strikingly illustrated by Fig. 3 in Ref. [16] for the bisectoral case).

This result (35), applied to Eq. (34b), entails that the observance of planar degeneracy is plainly equivalent to the assertion that the three-gluon coupling can be uniquely defined, irrespectively of the chosen kinematics, when the subtraction scale is fixed for the Bose-symmetric s invariant. Although approximate, this is a remarkable result.

In the following, we use a large-statistics set of quenched lattice-QCD configurations for multiple β's (described in Table I) and investigate further the validity of the planar degeneracy by extending previous results [73,74] to general kinematics, i.e., any set of lattice momenta (q, r, p) satisfying $q + r + p = 0$, corresponding to the white area in Fig. 2.

The large amount of lattice momenta for these general kinematics[5] will allow us (i) the scrutiny of possible effects due to lattice discretization artifacts associated to the breaking of the rotational invariance [94–96]; (ii) those beyond the planar degeneracy, i.e., residual dependencies either in t,u in Eqs. (13b) and (13c) or in the angles θ_{qr} and θ_{qp}; and, finally, (iii) to capitalize on the information for all the orbits to gain some physical insights into the three-gluon vertex running in its nonperturbative regime.

[4]Only an exploratory study, over a reduced number of non-bisectoral kinematics configuration, has been made so far confirming the observation of the property [16,73].

[5]For a N^4 lattice with $N = 32$, and limiting the momenta ($p = \frac{2\pi}{Na} n$) to $n \leq N/4$ to minimize the impact of lattice artifacts, there are 74 800 sets of momenta for the general kinematics, 1400 for the bisectoral, and only 32 and 64 for the symmetric and soft-gluon, respectively.

A. $H4$ dependence

It is well known that any given two-point lattice-regularized Green function, e.g., the gluon propagator, owing to the breaking of rotational $O(4)$ down to permutation $H(4)$ group invariance, depends on the four $H(4)$ invariants [94–97]

$$q^{[2n]} = \sum_{\mu=1}^{4} q_\mu^{2n} \tag{36}$$

with $n = 1,\ldots,4$; although only the dependence on $q^{[2]} \equiv q^2$ survives in the continuum limit: Clearly, $q^{[2n]}/q^2 \sim a^{2(n-1)} \to 0$. Thus, the dominant subleading contribution when the continuum limit is approached comes with $q^{[4]}$. A procedure, usually dubbed $H(4)$ extrapolation [94–97], has been developed and proven to be notably efficacious to cure two-point Green's functions from the $O(4)$-breaking lattice artifacts [16,73,78,86,98–102].

In three-point cases, as the three-gluon vertex, a lattice-regularized Green's function could generally depend on any $H(4)$ invariants that can be built with three momenta. The choice of a Bose-symmetric tensor basis implies for the corresponding form factors their depending only on Bose-symmetric combinations of $H(4)$ invariants, the dominant subleading contribution coming with

$$s^{[4]} = \frac{q^{[4]} + r^{[4]} + p^{[4]}}{4} \tag{37a}$$

$$= \frac{1}{2}\sum_{\mu=1}^{4} q_\mu^2 r_\mu^2 + q_\mu^2 p_\mu^2 + p_\mu^2 r_\mu^2. \tag{37b}$$

Other $H(4)$ invariants of a^4 dimensions can be also expressed in terms of $s^{[4]}$, as is made apparent by (37b).

Thus far, the $H(4)$ extrapolation has been successfully applied only for the three-point Green's functions in the soft-gluon case, in which only one momentum scale survives, and, concerning the kinematic analysis, it behaves as a two-point case [16,64–66,70,73], while, in the symmetric three-gluon case, the number of exploited kinematic configurations made unfeasible any detailed analysis of $O(4)$-breaking artifacts.

In this work, we capitalize on the statistical power for general kinematics and perform a first analysis of the impact of these artifacts on the three-gluon vertex. The main outcome of the analysis is illustrated by Fig. 3, which delivers the tree-level form factor $\bar{\Gamma}^*_1(q^2, p^2)$ for the bisectoral case in terms of $\theta_{qr} = 2(\pi - \theta_{qp})$ and for a given s^2, while the value of the $H(4)$-invariant $s^{[4]}$ appears indicated by a color scale. Namely, no sizable and systematic effect of $s^{[4]}$ appears on the tree-level form factor, as all data for almost each angle are, in practice, compatible within the errors. Otherwise expressed, a linear slope in $s^{[4]}$ computed for almost each angle is compatible with zero. In the cases shown in the figure, the

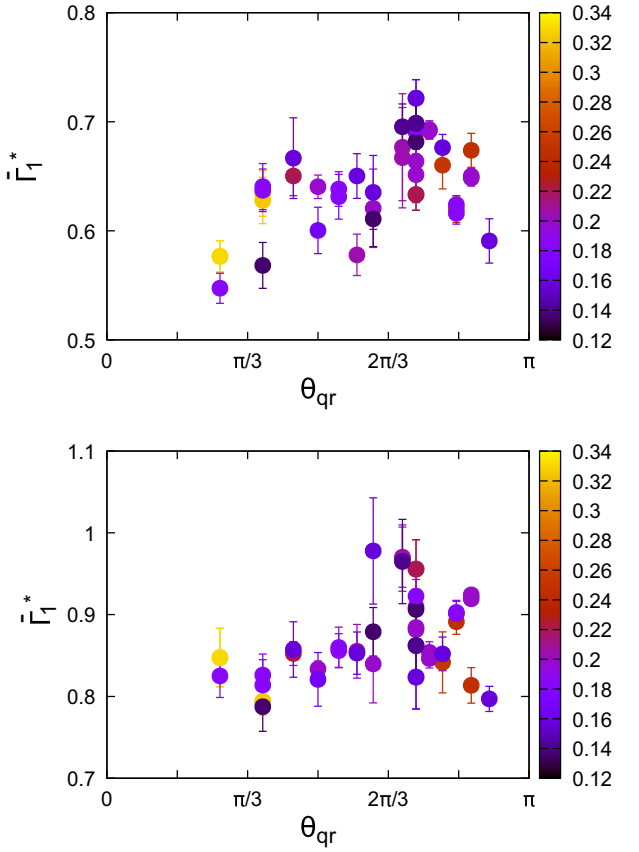

FIG. 3. The tree-level form factor for bisectoral kinematics ($q^2 = r^2$) displayed in terms of the angle θ_{qr}, for a fixed value of the Bose-symmetric invariant. Two illustrative cases are displayed, with $s^2 = 48a^{-2}(\beta)$ from two different lattice setups at $\beta = 5.8$ (top) and $\beta = 6.0$ (bottom). The color scale refers to the dimensionless ratio $s^{[4]}/(s^2)^2$.

slopes averaged over all the angles[6] are 0.09(13) and −0.03(16) for $\beta = 5.8$ and 6.0, respectively. It should be also highlighted that both the results' errors and dispersion notably increase near the symmetric configuration, $\theta_{qr} = 2\pi/3$. This observation is explained by the fact that, projecting out the form factor, one needs to deal with the inversion of a matrix, Eq. (10), whose determinant approaches zero near the symmetric configuration, due to dimensional reduction [73].

These findings are systematically observed for the different β's, any value of s^2, and all the kinematic configurations. Therefore, with the available statistical errors (corresponding to 2000 gauge-field configurations), it can be concluded that the lattice $O(4)$-breaking artifacts are not relevant, and, consequently, one can reliably average all the data that differ only in $s^{[4]}$ or other higher-order $H(4)$ invariants.

[6]Planar degeneracy makes the average significant, as it entails that the slope in $s^{[4]}$ is then independent of the angle.

B. Planar degeneracy

The planar degeneracy exhibited by the three-gluon tree-level form factor in a Bose-symmetric tensor basis can be mathematically expressed as

$$\tilde{\Gamma}^*_1(q^2, r^2, p^2; a) = \bar{\Gamma}^{\rm sg}(s^2; a), \tag{38}$$

in terms of bare quantities, which can be next renormalized in Rs, the soft-gluon MOM scheme, to recast (38) as

$$\tilde{\Gamma}^*_{1\,Rs(\zeta)}(q^2, r^2, p^2) = \bar{\Gamma}^{\rm sg}_R(s^2) = \frac{\bar{\Gamma}^{\rm sg}(s^2; a)}{\bar{\Gamma}^{\rm sg}(\zeta^2; a)}. \tag{39}$$

This is what Fig. 4 shows from our lattice QCD calculation with the Landau-gauge field configurations described in Table I. Therein, we average the results for Eq. (39)'s lhs (here, and in what follows, we take $\zeta = 4.3$ GeV) from all the available general nonbisectoral configurations sharing the same s invariant [i.e., those evaluated at k(s) with any available $\theta_{qp} \neq \theta_{rp}$] for each β; although we choose to display all with the same symbols (golden filled circles), in order to make the scaling more apparent. The tiny errors, evaluated as the mean squared width for the distribution of values at a given s, stem from their almost negligible dispersion and prove that Eq. (39)'s lhs does depend only on s^2 and not on the angles. On top of this, the outputs for bisectoral [blue: k(s) with any available $\theta_{qp} = \theta_{rp}$], symmetric [red: k($s$) with $\theta_{qp} = \theta_{rp} = 2\pi/3$], and soft-gluon [black: k(s) with $\theta_{qp} = \theta_{rp} = \pi/2$] are also displayed. The remarkable coincidence of all the results proves the equality expressed by Eq. (39) and, hence, planar degeneracy within the exposed kinematic range up to ∼4–5 GeV. It is worthwhile stressing the nice scaling achieved with six lattice setups, a different value of β each, represented all together in Fig. 4 for all kinematical configurations.

Then, we focus on the bisectoral case, considering four bins of momenta defined by a narrow interval around $s = 1$, 2, 3, and 4 GeV, respectively, and display them in terms of the angle $\theta_{qr} = 2(\pi - \theta_{rp})$ in the four panels in Fig. 5. Equation (38) establishes that, for each bin, the outputs should take the same value, which is referred to the soft-gluon case. This is what the four panels show, where the special soft-gluon and symmetric cases appear differentiated in black and red, respectively.

Planar degeneracy implies equivalent features for the form factors in any Bose-symmetric tensor basis, particularly, for those associated to the basis (6), $\tilde{\Gamma}_1$, which relates to $\tilde{\Gamma}^*_1$ as expressed in Eq. (12). The results for $\bar{\Gamma}_1$ and $\bar{\Gamma}^*_1$, which derive from $\tilde{\Gamma}_1$ and $\tilde{\Gamma}^*_1$ in the bisectoral case, are shown in Fig. 5 (the former in gray), and their comparison made apparent that, when the soft-gluon limit is approached and s^2 increases, the latter respects better the planar degeneracy than the former. The declining of $\bar{\Gamma}_1$ when $\theta_{qr} \to \pi$ is understood as caused by a perturbative

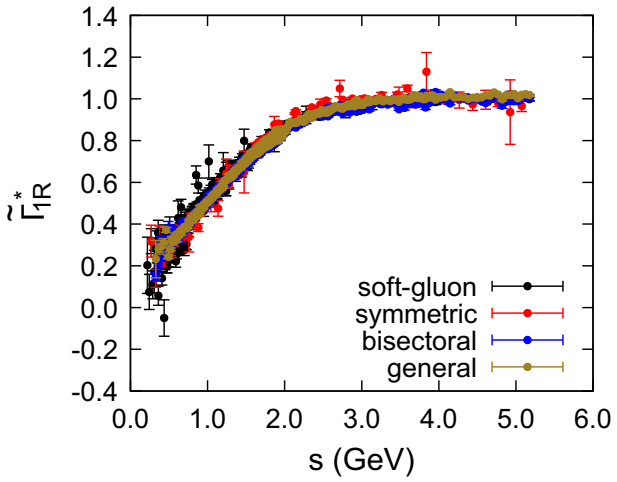

FIG. 4. The tree-level form factor evaluated at any kinematic configuration (q^2, r^2, p^2) and renormalized at the soft-gluon point $s(\zeta)$, Eq. (39)'s lhs, obtained from all the lattice configurations in Table I, the $O(4)$-breaking artifacts treated as explained in the text. We have taken $\zeta = 4.3$ GeV. The results for all available (non)bisectoral configurations evaluated at the same value of s^2 have been averaged for each value of β, as explained in the text, and all displayed with solid (golden) blue circles. The symmetric and soft-gluon cases are particularly shown in red and black, respectively.

singularity in this limit [16], which can be nonperturbatively removed [53] but spoils increasingly the constant behavior imposed by Eq. (39) when s^2 grows up. This perturbative singularity also enters in $\bar{\Gamma}_3$ canceling that of $\bar{\Gamma}_1$ when they are combined[7] as in Eq. (12), thereby resulting in $\bar{\Gamma}^*_1$ which delivers by itself the correct soft-gluon limit [see Eq. (23)].

All these results, obtained from lattice gauge-field configurations, are plainly consistent with the analysis based on a continuum DSE calculation of the three-gluon vertex in Ref. [53]. As an illustration of this excellent agreement, we have included in every panel in Fig. 5 the DSE result for $\bar{\Gamma}^*_1$ and $\bar{\Gamma}_1$ obtained at the corresponding value of s^2 as explained in Ref. [53].

Concerning the other two form factors, $\bar{\Gamma}^*_2$ and $\bar{\Gamma}^*_3$, again derived from $\tilde{\Gamma}^*_2$ and $\tilde{\Gamma}^*_2$ as given by Eq. (18) and, according to Eq. (12), equivalent to $\bar{\Gamma}_2$ and $\bar{\Gamma}_3$, we found them almost compatible with zero, within errors, and negligible thereby, as claimed in Ref. [73]. They are plotted in Figs. 6 and 7, respectively, for $s = 1$ and 4 GeV. It can be therein noticed that the only sizable nonzero contribution, but very small compared to $\bar{\Gamma}^*_1$, takes place for $\bar{\Gamma}^*_3$ in the soft-gluon limit ($\theta_{qr} = \pi$) when s becomes large. Indeed, this contribution to $\bar{\Gamma}^*_3 \equiv \bar{\Gamma}_3$ explains why $\bar{\Gamma}^*_1$ and $\bar{\Gamma}_1$ differ from each other in that kinematic domain, canceling out the effect of the

[7]They are indeed combined by an equation which results from applying Eq. (18) to (12) and which, as $f^*_1 = f_1 + 3/2 f_3$, appears to be the same restricted to $d = 3$.

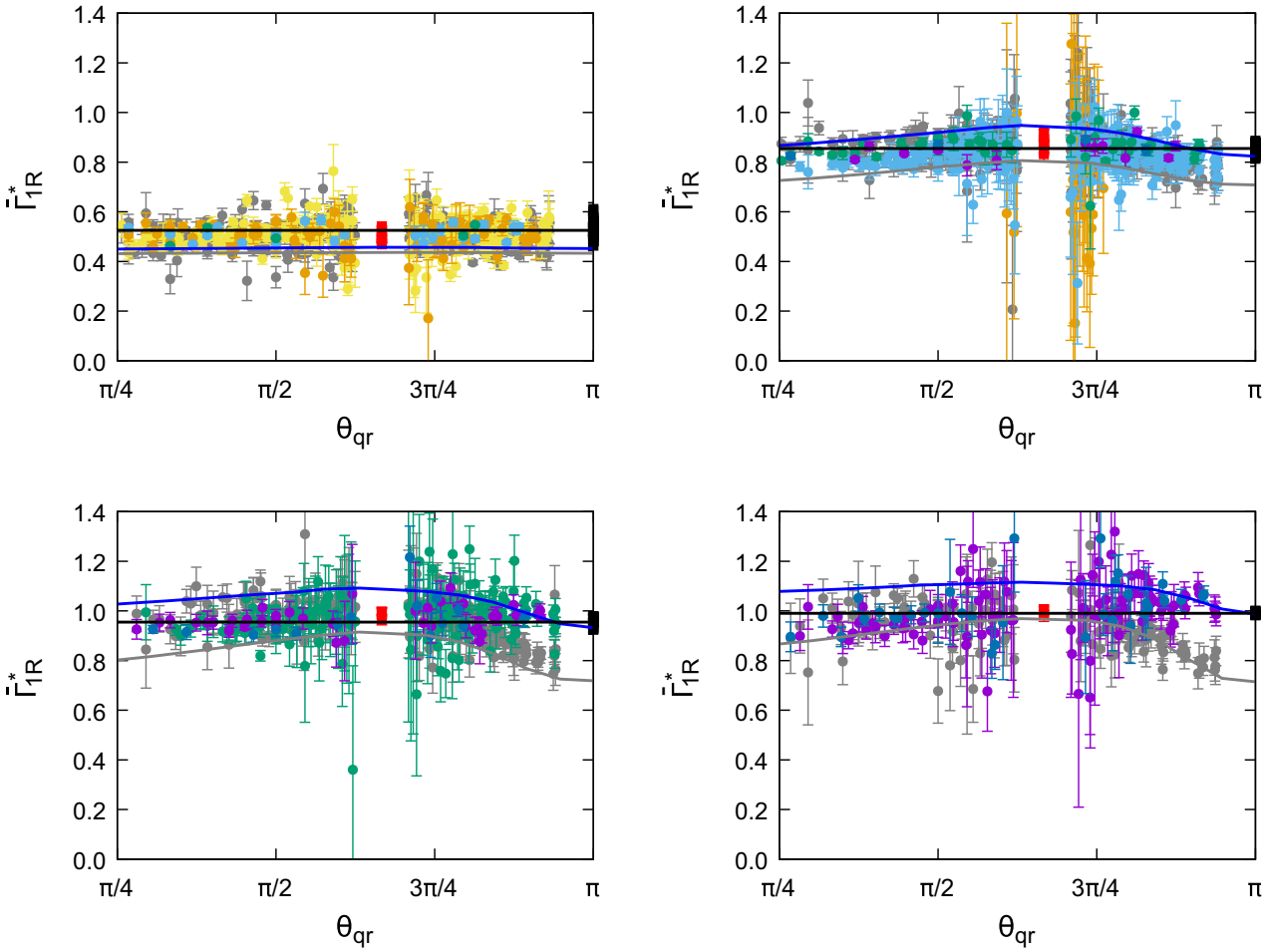

FIG. 5. The tree-level form factor $\bar{\Gamma}_1^*(q^2, p^2)$ for bisectoral kinematics ($q^2 = r^2$) renormalized as in Eq. (30), at the soft-gluon point $s(\zeta)$ with $\zeta = 4.3$ GeV, as a function of the angle between equal momenta, θ_{qr}, for fixed values of s: from left to right 1 and 2 (top) and 3 and 4 GeV (bottom). The results obtained from lattice configurations with different β's are displayed in different colors: $\beta = 5.6$ (yellow), 5.7 (orange), 5.8 (light blue), 6.0 (green), 6.2 (purple), and 6.4 (dark blue). The same for $\bar{\Gamma}_1(q^2, p^2)$ is shown in gray, thus to expose the advantage of using the tensor basis (11) instead of (6), basically at large s and θ_{qr} near π (soft-gluon). Results for values of θ_{qr} near $2\pi/3$ (symmetric) have been eliminated for clarity, as they are affected by the numerical noise induced by that one of matrix (10)'s eigenvalues approaches zero. The soft-gluon (symmetric) case is plotted in black (red) for all β's. The average of soft-gluon results is also displayed by a dot-dashed black line. The DSE results obtained as discussed in Ref. [53] appear displayed in each panel, at its corresponding value of s with a dashed blue (solid gray) line for $\bar{\Gamma}_1^*$ ($\bar{\Gamma}_1$).

perturbative singularity in $\bar{\Gamma}_1$ and restoring the planar degeneracy as an excellent approximation for $\bar{\Gamma}_1^*$.

Although choosing to display the bisectoral case, in which they depend only on a single angle, making thus easier the representation, we have checked that $\bar{\Gamma}_2^*$ and $\bar{\Gamma}_3^*$ are negligible beyond, in any general kinematic configuration. Clearly, this implies the same also for $\tilde{\Gamma}_2^*$, $\tilde{\Gamma}_3^*$, and $\tilde{\Gamma}_4^*$ or, otherwise, according to Eq. (18), a very delicate and implausible cancellation needs to involve the latter with the two former ones. Furthermore, we have calculated $\tilde{\Gamma}_4^*$ and concluded that, albeit noisier than the other form factors, it is compatible with zero in general kinematics.

Altogether, our findings support that one can very accurately approximate the transversely projected three-gluon vertex by

$$\bar{\Gamma}_{R\alpha\mu\nu}(q, r, p) = \bar{\Gamma}_R^{\mathrm{sg}}(s^2)\tilde{\lambda}_{1\alpha\mu\nu}(q, r, p), \tag{40}$$

renormalized at a subtraction point defined only by $s^2 = \zeta^2$, irrespectively of the angles or, alternatively, the two other Bose-symmetric invariants.

C. Zero crossing and logarithmic singularity

The key ingredient defining the transversely projected three-gluon vertex, according to Eq. (40), is the soft-gluon form factor $\bar{\Gamma}^{\mathrm{sg}}$. Thus far, we have carefully scrutinized the tree-level form factor $\bar{\Gamma}_1^*$ and proved that planar degeneracy works remarkably well to describe its behavior for any general kinematic configuration within the exposed range. At this point and in the following, we assume planar

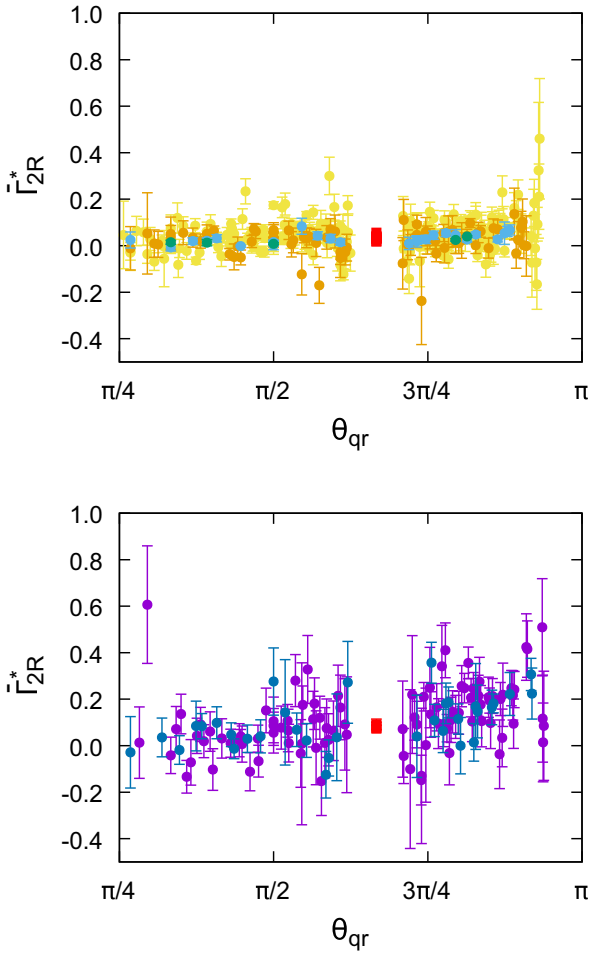

FIG. 6. The form factor $\bar{\Gamma}^*_2(q^2, p^2)$ for bisectoral kinematics ($q^2 = r^2$), renormalized as in Eq. (30) at the soft-gluon point s(ζ) with $\zeta = 4.3$ GeV, for the two fixed values $s = 1$ and 4 GeV (legends as in Fig. 5). The results for the symmetric point are shown in red, and, as in Fig. 5, results for θ_{qr} near $2\pi/3$ are removed to avoid numerical noise. The soft-gluon result ($\theta_{qr} = \pi$) does not exist as the corresponding basis tensor $\bar{\lambda}^*_{2\alpha\mu\nu}$ vanishes in this limit; while, in the symmetric case ($\theta_{qr} = 2\pi/3$), the output is a combination of the limits for $\bar{\Gamma}^*_2(q^2, p^2)$ and $\bar{\Gamma}^*_3(q^2, p^2)$ [viz. Eq. (21)]. The form factor $\bar{\Gamma}_2(q^2, p^2)$, associated to the basis (6), is identical to $\bar{\Gamma}^*_2(q^2, p^2)$, according to (12).

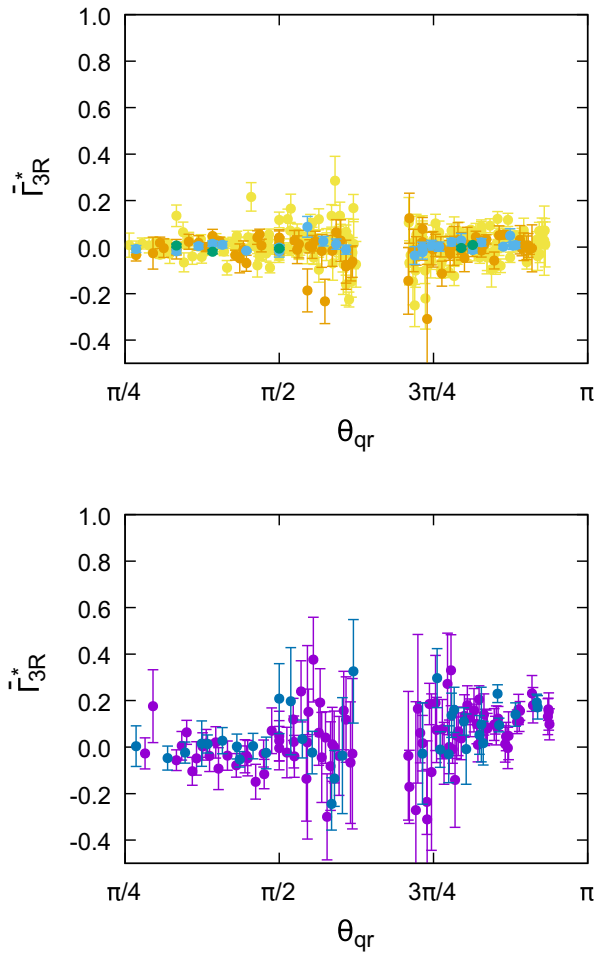

FIG. 7. The same as Fig. 6, here for $\bar{\Gamma}^*_3(q^2, p^2)$. In this case, neither the soft-gluon nor the symmetric cases exist, because, according to Eq. (21), the basis tensor $\bar{\lambda}^*_{3\alpha\mu\nu}$ projects into the soft-gluon limit of $\bar{\lambda}^*_{1\alpha\mu\nu}$ or into the symmetric limits of $\bar{\lambda}^*_{1\alpha\mu\nu}$ and $\bar{\lambda}^*_{2\alpha\mu\nu}$.

degeneracy and recalculate $\bar{\Gamma}^{\rm sg}$ from lattice QCD by capitalizing on our large-statistics sample of gauge configurations, as an average over the many different kinematic configurations $k(s)$, for all available angles θ_{qp} and θ_{qr} at each value of the Bose-symmetric invariant s.

Figure 8 shows the lattice results for $\bar{\Gamma}^{\rm sg}_R$ and displays also a best fit with an expression motivated by a construction of the three-gluon vertex relying on the STIs that it satisfies [52,66,67,71], Eqs. (A6) and (A10) in the Appendix. A main feature of the three-gluon vertex revealed by this construction, and confirmed by lattice analyses [64,65,68], is the presence of an infrared zero crossing at very low values of s induced by a logarithmic divergence at vanishing momenta. This singularity plays an important dynamical role, as it is caused by the interplay of massless ghosts and massive gluons in the loops of the three-gluon DSE expansion [51] and can be related to the dynamical gluon mass generation [10,11] at the level of the two-point function via the corresponding STI [52] (see the Appendix).

Our best fit over the ensemble of lattice data leaves us with a global determination for the zero-crossing location, as shown in Table II. However, the fitting expression behaves as

$$\bar{\Gamma}^{\rm sg}_R(s^2) = \gamma_0 + \gamma_1 \ln\left(\frac{s^2}{\zeta^2}\right), \tag{41}$$

at asymptotically low s, with $\gamma_1 = 0.11$ [viz. Eq. (A11)]. Indeed, Eq. (41) is the more general output from identifying and linking via STI the two- and three-point singularities

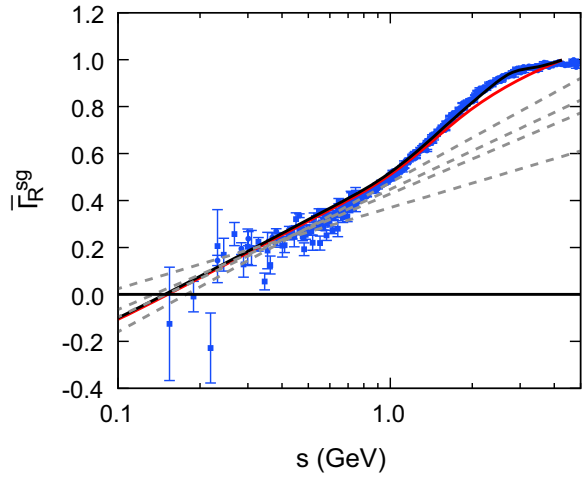

FIG. 8. Semi-log plot of the form factor $\bar{\Gamma}^{sg}_R$ evaluated, as explained in the text, by assuming planar degeneracy and averaging for all kinematic configurations at fixed s^2. The fit given in Ref. [67] [viz. Eq. (A6)] is displayed in a solid red line, while the refined version herein introduced [viz. Eq. (A10)] is in black; and the fits with Eq. (41) described in Table II are depicted with dashed gray lines.

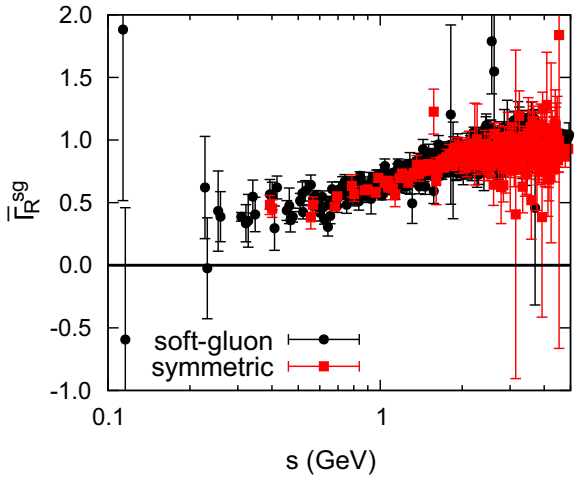

FIG. 9. The tree-level form factor renormalized at the soft-gluon point $s(\zeta)$ with $\zeta = 4.3$ GeV, Eq. (39)'s lhs, obtained from $\bar{\Gamma}^{sym}_1$ and $\bar{\Gamma}^{sg}$ [see Eqs. (21) and (22)], calculated with unquenched $N_F = 2+1$ lattice configurations at a physical pion mass [70], and here expressed in terms of the Bose-symmetric invariant s^2.

generated by massless ghosts [11,103]. The same can be also concluded from other approaches for the description of the low-momentum behavior of QCD Green's functions [104]. Therefore, in the aim of estimating a systematic uncertainty for the zero-crossing location, we fit Eq. (41) with free parameters to all the lattice data below a given scale s_{max}, ranging from 0.4 to 0.7 GeV, and derive thereby the location from the fitted parameters: $s_0 = \zeta \exp(-\gamma_0/[2\gamma_1])$. The results can be found in Table II, and the corresponding fits appear displayed in Fig. 8. It should be noticed that the slope gets smaller for smaller fitting windows, likely indicating that the uncertainty for a lower zero-crossing location value is underestimated.

The tree-level form factor has been formerly analyzed in both the particular cases of symmetric and soft-gluon kinematics [70], by using a set of $N_F = 2+1$ DWF unquenched gauge-field lattice configurations at a physical pion mass, to unveil any possible effect from realistic dynamical quarks. Then, we capitalize on the results of Ref. [70] to test and confirm that planar degeneracy works equally well in the unquenched case, by displaying them in terms of the Bose-symmetric invariant s in Fig. 9: Lattice data for the tree-level form factor in the two different kinematic cases, both renormalized at the same subtraction point, exhibit an almost perfect overlapping within errors. As for the quenched case, the agreement is indeed perfect within the IR domain and up to roughly 4 GeV, some marginal discrepancies appearing above which should rely on the distinct perturbative running for different kinematics.

Finally, the four panels in Fig. 5 made strikingly apparent the validity of Eq. (38) from our lattice calculation and, hence, (35). The DSE results therein displayed also confirms that this is a good approximation and, especially within the IR domain, becomes exact in practice (see the first panel for $s = 1$ GeV). We can therefore conclude that, in very good approximation, a unique three-gluon coupling

$$\alpha_{3g}(\zeta^2) = \frac{g^2_{Rk}(\zeta^2)}{4\pi} \equiv \frac{g^2_{Rs}(\zeta^2)}{4\pi} \tag{42}$$

results from (34), the subtraction point fixed at $s^2 = \zeta^2$ for any kinematic configuration. This is shown in Fig. 10, where our lattice data display this unique three-gluon coupling behavior for momenta below ∼4 GeV. At this point, we can recall the instructive discussion in the end of Sec. IV in Ref. [67], where the effective strength associated to gluon-gluon interaction was compared to ghost-gluon by using the coupling (42) in the soft-gluon renormalization scheme. Our result here, inferred from the observance of the three-gluon planar degeneracy, entails that this is the unique effective strength for the gluon-gluon interaction from the three-gluon coupling.

TABLE II. Logarithmic slope γ_1 and zero-crossing location s_0 for different fitting windows and combining data for all the kinematics and lattice setups. The last row corresponds to the results from the best fit of Eq. (A10) to all data.

s_{max} (GeV)	γ_1	s_0 (MeV)
0.7	0.138(2)	178(3)
0.6	0.118(6)	150(9)
0.5	0.107(16)	135(23)
0.4	0.075(23)	85(38)
⋯	0.11	161

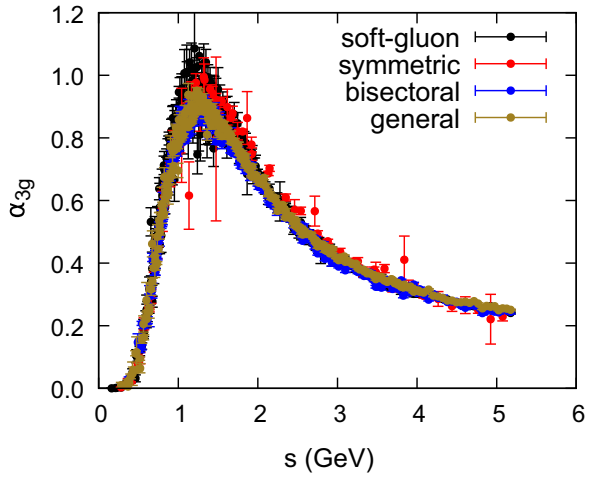

FIG. 10. Strong effective coupling defined by Eq. (42) and obtained according to Eq. (34) for all kinematics as done (and labeled) in Fig. 4.

IV. CONCLUSIONS

In the present investigation of the Landau-gauge three-gluon vertex from lattice QCD, we have aimed at the completion of a series of previous works by the study of the full kinematic range and tensor space available to the transversely projected vertex.

Two different Bose-symmetric basis have been considered, both including the tree-level (classical) tensor as one of their elements. The first basis is the one implemented in the previous lattice study [73], while the second one [53] is built by rearranging the tensors of the first basis, only entailing a minimal modification of the form factor associated to the classical one. This classical form factor becomes then improved, as it fully contains the three-gluon vertex in the soft-gluon limit. In both cases, the corresponding form factors have been projected out from the three-gluon Green's function and, evaluating carefully the impact of $O(4)$-breaking lattice artifacts, have been seen to (i) be dominated by the classical form factor, which (ii) is furthermore shown to depend only on the Bose-symmetric combination of momenta s^2 [viz. Eq. (13a)], for $s \leq 4$–5 GeV. The latter being true in practice after the implementation of the two basis, a very small violation of (ii) in the vicinity of the soft-gluon limit and growing up with the momentum appears to be eliminated by the improved version of the basis. These results deliver an important confirmation, for a fully general three-gluon vertex, of the property unveiled in previous works and termed planar degeneracy. We have furthermore presented the first evidence for this phenomenon in realistic QCD, beyond pure Yang-Mills, by exploiting unquenched gauge-field configurations using DWF at a physical pion mass.

Finally, we have deepened into the implications of this remarkable property and have shown that the transversely projected three-gluon vertex can be uniquely renormalized in the MOM scheme, irrespectively of the chosen kinematic configuration, when the subtraction point is defined at a given value of the Bose-symmetric combination s^2 [viz. Eq. (40)]. Thus, this renormalized vertex can be expressed in terms of the only form factor in the soft-gluon case which, capitalizing on the planar degeneracy, can be very accurately displayed by considering all the lattice data for all kinematic configurations (viz. Fig. 8). Finally, an effective coupling can be also defined [viz. Eq. (42)], relying on this unique MOM three-gluon vertex, as a sensible expression of the gluon-gluon interaction strength.

ACKNOWLEDGMENTS

We are grateful to A. C. Aguilar, M. N. Ferreira, and J. Papavassiliou, for the fruitful discussions that gave rise to some of the ideas exposed in this work and for providing us with the DSE results displayed for comparison in Fig. 5. F. P.-G. also thanks A. C. Aguilar for her warm hospitality and support and Banco Santander for partially financing this work. The work has been funded by the Spanish "Ministerio de Ciencia e Innovación (MICINN)" through Grants No. PID2019-107844-GB-C22 and No. PID2022-140440-NB-C22. The authors acknowledge the C3UPO of the Pablo de Olavide University for the support with HPC facilities.

APPENDIX: THE THREE-GLUON STIS AND THE TREE-LEVEL FORM FACTOR

As discussed in, e.g., Ref. [66], one can generally write the 1PI three-gluon vertex as

$$\mathrm{I}\Gamma^{\alpha\mu\nu}(q,r,p) = V^{\alpha\mu\nu}(q,r,p) + \Gamma^{\alpha\mu\nu}(q,r,p), \tag{A1}$$

$$\Gamma^{\alpha\mu\nu}(q,r,p) = \sum_{i=1}^{10} X_i(q^2,r^2,p^2)\mathscr{C}_i^{\alpha\mu\nu} + \sum_{j=1}^{4} Y_j(q^2,r^2,p^2)t_j^{\alpha\mu\nu}, \tag{A2}$$

where $V^{\alpha\mu\nu}$ contains the longitudinally coupled Schwinger poles while, resorting to the Ball-Chiu basis [8,84] [see, e.g., Eqs. (3.4) and (3.6) in Ref. [52]], the free-pole part $\Gamma^{\alpha\mu\nu}$ is decomposed into two, transverse and nontransverse, pieces. One can then capitalize on the STIs involving the three-gluon vertex, namely,

$$p_\nu \mathrm{I}\Gamma^{\alpha\mu\nu}(q,r,p) = F(p^2)[\mathcal{T}^{\mu\alpha}(r,p,q) - \mathcal{T}^{\alpha\mu}(q,p,r)], \tag{A3}$$

with $F(p^2)$ standing for the ghost dressing function and $\mathcal{T}^{\alpha\mu}$ for a tensor structure involving the gluon propagator and the ghost-gluon scattering kernel [8,9,105], and rely on Eq. (A3)'s rhs for the construction of the nontransverse

components resulting from the vertex contraction in (A3)'s lhs.

Rooting on the Schwinger mechanism for the generation of a dynamical gluon mass, the gluon propagator can be written as[8]

$$[\Delta(p^2)]^{-1} = p^2 J(p^2) + m^2(p^2); \tag{A4}$$

and it can be proven that, in (A3), the dynamical gluon mass $m^2(p^2)$ is attached only to $V^{\alpha\mu\nu}$ and the kinetic term $J(p^2)$ to the nontransverse piece of $\Gamma^{\alpha\mu\nu}$ [10,11]. Notwithstanding this decoupling of $m^2(p^2)$ and $J(p^2)$ at the level of the STIs, they remain coupled by the gluon propagator DSE, in which the full three-gluon vertex enters and triggers the Schwinger mechanism.

The form factors X_i defined in Eq. (A3) can be thus derived from the STIs like (A3), being then particularly related to $F(p^2)$ and $J(p^2)$. This latter can be seen to receive the contribution of a logarithmic singularity caused by ghost loops in the DSE expansion of the gluon propagator which, contrarily to gluon loops, do not remain *protected* by a dynamically generated mass [51]. The same happens for the form factors X_i, which are impacted by a logarithmic singularity of the same origin from the three-gluon vertex SDE. The STIs connect both singularities [52].

In this work, we calculate from lattice QCD the transversely projected three-gluon vertex, Eq. (2). For this, the contraction of the 1PI vertex with the transverse projectors mixes the transverse and nontransverse pieces of Eq. (A2) and makes the form factors in the Bose-symmetric tensor basis, either (6) or (11), depend on different combinations of X_i and Y_i. However, although the form factors Y_i cannot be extracted from the STIs, one is specially left with [67]

$$\bar{\Gamma}^{\mathrm{sg}}(q^2) = X_1(q^2, q^2, 0) - q^2 X_3(q^2, q^2, 0), \tag{A5}$$

in the soft-gluon case. Consequently, on the basis of the planar degeneracy approximation and within its validity momentum range, the transversely projected vertex remains completely defined by the STIs.

The knowledge of $J(p^2)$ is required, and it derives from the gluon propagator DSE which, in its turn, involves the three-gluon vertex (A1). Given the complexity of solving the gluon propagator DSE *in its full glory*, an approximate iterative procedure resorting to the dynamical equation for $m^2(p^2)$ [71] and to gluon propagator lattice data is described and followed in Ref. [66]. Relying on this output for $J(p^2)$, the STI-based construction of $\bar{\Gamma}^{\mathrm{sg}}$ appears to be in good agreement with the lattice data therein delivered for the soft-gluon case. In Ref. [67], the STI-based result for $\bar{\Gamma}^{\mathrm{sg}}$ is accurately fitted to

$$R(p^2) = F(p^2)T(p^2) + \nu_1\left(\frac{1}{1+(p^2/\nu_2)^2} - \frac{1}{1+(\zeta^2/\nu_2)^2}\right); \tag{A6}$$

$R(p^2)$ being a functional form inspired by the STI construction of the vertex, with $\nu_{1,2} = 0.165$ and $0.83\ \mathrm{GeV}^2$ and where

$$T(p^2) = 1 + \frac{3\lambda_s}{4\pi}\left(1 + \frac{\tau_{1s}}{\tau_{2s}+p^2}\right) \times \left[2\ln\frac{p^2+\eta_s^2(p^2)}{\zeta^2+\eta_s^2(\zeta^2)} + \frac{1}{6}\ln\frac{p^2}{\zeta^2}\right] \tag{A7}$$

and

$$F^{-1}(p^2) = 1 + \frac{9\lambda_F}{16\pi}\left(1+\frac{\tau_{1F}}{\tau_{2F}+p^2}\right)\ln\frac{p^2+\eta_F^2(p^2)}{\zeta^2+\eta_F^2(\zeta^2)} \tag{A8}$$

dominate the low-momentum behavior and are determined by the best fits to the solution of $J(p^2)$ and to ghost dressing lattice data, respectively, with

$$\eta_{s,F}^2(p^2) = \frac{\eta_{1s,F}^2}{1+p^2/\eta_{2s,F}^2}. \tag{A9}$$

The parameters for Eqs. (A7) and (A8) are [67] $\lambda_s = 0.27$, $\tau_{1s} = 2.67, \tau_{2s} = 1.05, \eta_{1s}^2 = 3.10, \eta_{2s}^2 = 0.729$; $\lambda_F = 0.22$, $\tau_{1F} = 6.34$, $\tau_{2F} = 2.85$, $\eta_{1F}^2 = 0.107$, and $\eta_{2F}^2 = 11.2$; all parameters are in units of GeV^2, except the dimensionless $\lambda_{s,F}$.

In this work, we deliver a very precise lattice prediction of the soft-gluon form factor based on planar degeneracy and on exploiting thereby all available kinematic configurations. Consequently, we need to slightly refine the fitting expression, now reading

$$\bar{\Gamma}_R^{\mathrm{sg}}(p^2) = R(p^2) + \frac{\nu_3}{1+[(p^2-p_0^2)/\nu_4]^2} - \frac{\nu_3}{1+[(\zeta^2-p_0^2)/\nu_4]^2}, \tag{A10}$$

and can thus deliver a very accurate description of our prediction with $p_0 = 2.7\ \mathrm{GeV}$ and $\nu_{3,4} = 0.054$ and $4.12\ \mathrm{GeV}^2$, for all momenta below the subtraction point $\zeta = 4.3\ \mathrm{GeV}$. It is worthwhile to remark that the low-momentum asymptotic behavior reads

$$\bar{\Gamma}_R^{\mathrm{sg}}(p^2) \sim F(0)\frac{\lambda_s}{8\pi}\left(1+\frac{\tau_{1s}}{\tau_{2s}}\right)\ln\frac{p^2}{\zeta^2} = 0.11\ln\frac{p^2}{\zeta^2}, \tag{A11}$$

fully relying on Eqs. (A7) and (A8) and on the DSE determinations of the two-point gluon and ghost Green's functions from Refs. [66,67].

[8]The dependence on the renormalization scale ζ^2 is kept implicit.

[1] S. L. Glashow, Partial symmetries of weak interactions, Nucl. Phys. **22**, 579 (1961).
[2] Steven Weinberg, A model of leptons, Phys. Rev. Lett. **19**, 1264 (1967).
[3] Abdus Salam, Weak and electromagnetic interactions, eConf **C680519**, 367 (1968).
[4] David J. Gross and Frank Wilczek, Ultraviolet behavior of non-Abelian gauge theories, Phys. Rev. Lett. **30**, 1343 (1973).
[5] H. David Politzer, Reliable perturbative results for strong interactions?, Phys. Rev. Lett. **30**, 1346 (1973).
[6] Craig D. Roberts, Hadron structure using continuum Schwinger function methods, Few-Body Syst. **64**, 51 (2023).
[7] William J. Marciano and Heinz Pagels, Quantum chromodynamics: A review, Phys. Rep. **36**, 137 (1978).
[8] James S. Ball and Ting-Wai Chiu, Analytic properties of the vertex function in gauge theories. 2, Phys. Rev. D **22**, 2550 (1980).
[9] Andrei I. Davydychev, P. Osland, and O. V. Tarasov, Three-gluon vertex in arbitrary gauge and dimension, Phys. Rev. D **54**, 4087 (1996).
[10] D. Binosi, D. Ibañez, and J. Papavassiliou, The all-order equation of the effective gluon mass, Phys. Rev. D **86**, 085033 (2012).
[11] A. C. Aguilar, D. Ibáñez, V. Mathieu, and J. Papavassiliou, Massless bound-state excitations and the Schwinger mechanism in QCD, Phys. Rev. D **85**, 014018 (2012).
[12] D. Ibáñez and J. Papavassiliou, Gluon mass generation in the massless bound-state formalism, Phys. Rev. D **87**, 034008 (2013).
[13] Daniele Binosi and Joannis Papavassiliou, Coupled dynamics in gluon mass generation and the impact of the three-gluon vertex, Phys. Rev. D **97**, 054029 (2018).
[14] Daniele Binosi, Emergent hadron mass in strong dynamics, Few-Body Syst. **63**, 42 (2022).
[15] J. Papavassiliou, Emergence of mass in the gauge sector of QCD, Chin. Phys. C **46**, 112001 (2022).
[16] A. C. Aguilar, F. De Soto, M. N. Ferreira, J. Papavassiliou, F. Pinto-Gómez, C. D. Roberts, and J. Rodríguez-Quintero, Schwinger mechanism for gluons from lattice QCD, Phys. Lett. B **841**, 137906 (2023).
[17] Julian S. Schwinger, Gauge invariance and mass, Phys. Rev. **125**, 397 (1962).
[18] Julian S. Schwinger, Gauge invariance and mass. 2, Phys. Rev. **128**, 2425 (1962).
[19] John M. Cornwall, Dynamical mass generation in continuum QCD, Phys. Rev. D **26**, 1453 (1982).
[20] R. Jackiw and K. Johnson, Dynamical model of spontaneously broken gauge symmetries, Phys. Rev. D **8**, 2386 (1973).
[21] E. Eichten and F. Feinberg, Dynamical symmetry breaking of non-Abelian gauge symmetries, Phys. Rev. D **10**, 3254 (1974).
[22] A. C. Aguilar, M. N. Ferreira, and J. Papavassiliou, Exploring smoking-gun signals of the Schwinger mechanism in QCD, Phys. Rev. D **105**, 014030 (2022).
[23] A. C. Aguilar, D. Binosi, and J. Papavassiliou, Gluon and ghost propagators in the Landau gauge: Deriving lattice results from Schwinger-Dyson equations, Phys. Rev. D **78**, 025010 (2008).
[24] Ph. Boucaud, J. P. Leroy, A. Le Yaouanc, J. Micheli, O. Pène, and J. Rodríguez-Quintero, On the IR behaviour of the Landau-gauge ghost propagator, J. High Energy Phys. 06 (2008) 099.
[25] Christian S. Fischer, Axel Maas, and Jan M. Pawlowski, On the infrared behavior of Landau gauge Yang-Mills theory, Ann. Phys. (N.Y.) **324**, 2408 (2009).
[26] J. Rodriguez-Quintero, On the massive gluon propagator, the PT-BFM scheme and the low-momentum behaviour of decoupling and scaling DSE solutions, J. High Energy Phys. 01 (2011) 105.
[27] M. R. Pennington and D. J. Wilson, Are the dressed gluon and ghost propagators in the Landau gauge presently determined in the confinement regime of QCD?, Phys. Rev. D **84**, 119901 (2011).
[28] Pieter Maris and Craig D. Roberts, Dyson-Schwinger equations: A tool for hadron physics, Int. J. Mod. Phys. E **12**, 297 (2003).
[29] A. C. Aguilar and A. A. Natale, A dynamical gluon mass solution in a coupled system of the Schwinger-Dyson equations, J. High Energy Phys. 08 (2004) 057.
[30] Christian S. Fischer, Infrared properties of QCD from Dyson-Schwinger equations, J. Phys. G **32**, R253 (2006).
[31] Kei-Ichi Kondo, Gauge-invariant gluon mass, infrared Abelian dominance and stability of magnetic vacuum, Phys. Rev. D **74**, 125003 (2006).
[32] Ph. Boucaud, Thorsten Brüntjen, Jean Pierre Leroy, Alain Le Yaouanc, Alexey Lokhov, Jacques Micheli, Olivier Pène, and Jose Rodriguez-Quintero, Is the QCD ghost dressing function finite at zero momentum?, J. High Energy Phys. 06 (2006) 001.
[33] Daniele Binosi and Joannis Papavassiliou, Gauge-invariant truncation scheme for the Schwinger-Dyson equations of QCD, Phys. Rev. D **77**, 061702 (2008).
[34] D. Binosi and J. Papavassiliou, New Schwinger-Dyson equations for non-Abelian gauge theories, J. High Energy Phys. 08 (2008) 063.
[35] Philippe Boucaud, J. P. Leroy, A. Le Yaouanc, A. Y. Lokhov, J. Micheli, O. Pene, J. Rodriguez-Quintero, and C. Roiesnel, Divergent IR gluon propagator from Ward-Slavnov-Taylor identities?, J. High Energy Phys. 03 (2007) 076.
[36] D. Dudal, S. P. Sorella, N. Vandersickel, and H. Verschelde, New features of the gluon and ghost propagator in the infrared region from the Gribov-Zwanziger approach, Phys. Rev. D **77**, 071501(R) (2008)..
[37] David Dudal, John A. Gracey, Silvio Paolo Sorella, Nele Vandersickel, and Henri Verschelde, A refinement of the Gribov-Zwanziger approach in the Landau gauge: Infrared propagators in harmony with the lattice results, Phys. Rev. D **78**, 065047 (2008).
[38] Matthieu Tissier and Nicolas Wschebor, Infrared propagators of Yang-Mills theory from perturbation theory, Phys. Rev. D **82**, 101701 (2010).
[39] Matthieu Tissier and Nicolas Wschebor, An infrared safe perturbative approach to Yang-Mills correlators, Phys. Rev. D **84**, 045018 (2011).
[40] Kei-Ichi Kondo, A low-energy effective Yang-Mills theory for quark and gluon confinement, Phys. Rev. D **84**, 061702 (2011).

[41] Adam P. Szczepaniak and Eric S. Swanson, Coulomb gauge QCD, confinement, and the constituent representation, Phys. Rev. D **65**, 025012 (2002).
[42] Adam P. Szczepaniak, Confinement and gluon propagator in Coulomb gauge QCD, Phys. Rev. D **69**, 074031 (2004).
[43] D. Epple, H. Reinhardt, W. Schleifenbaum, and A. P. Szczepaniak, Subcritical solution of the Yang-Mills Schroedinger equation in the Coulomb gauge, Phys. Rev. D **77**, 085007 (2008).
[44] Adam P. Szczepaniak and Hrayr H. Matevosyan, A model for QCD ground state with magnetic disorder, Phys. Rev. D **81**, 094007 (2010).
[45] Peter Watson and Hugo Reinhardt, The Coulomb gauge ghost Dyson-Schwinger equation, Phys. Rev. D **82**, 125010 (2010).
[46] Peter Watson and Hugo Reinhardt, Leading order infrared quantum chromodynamics in Coulomb gauge, Phys. Rev. D **85**, 025014 (2012).
[47] Attilio Cucchieri and Tereza Mendes, What's up with IR gluon and ghost propagators in Landau gauge? A puzzling answer from huge lattices, Proc. Sci. LAT2007 (**2007**) 297.
[48] I. L. Bogolubsky, E. M. Ilgenfritz, M. Muller-Preussker, and A. Sternbeck, Lattice gluodynamics computation of Landau gauge Green's functions in the deep infrared, Phys. Lett. B **676**, 69 (2009).
[49] O. Oliveira and P. J. Silva, The lattice infrared Landau gauge gluon propagator: The infinite volume limit, Proc. Sci. LAT2009 (**2009**) 226.
[50] A. Ayala, A. Bashir, D. Binosi, M. Cristoforetti, and J. Rodriguez-Quintero, Quark flavour effects on gluon and ghost propagators, Phys. Rev. D **86**, 074512 (2012).
[51] A. C. Aguilar, D. Binosi, D. Ibañez, and J. Papavassiliou, Effects of divergent ghost loops on the Green's functions of QCD, Phys. Rev. D **89**, 085008 (2014).
[52] A. C. Aguilar, M. N. Ferreira, C. T. Figueiredo, and J. Papavassiliou, Nonperturbative Ball-Chiu construction of the three-gluon vertex, Phys. Rev. D **99**, 094010 (2019).
[53] A. C. Aguilar, M. N. Ferreira, J. Papavassiliou, and L. R. Santos, Planar degeneracy of the three-gluon vertex, Eur. Phys. J. C **83**, 549 (2023).
[54] Attilio Cucchieri, Axel Maas, and Tereza Mendes, Exploratory study of three-point Green's functions in Landau-gauge Yang-Mills theory, Phys. Rev. D **74**, 014503 (2006).
[55] Attilio Cucchieri, Axel Maas, and Tereza Mendes, Three-point vertices in Landau-gauge Yang-Mills theory, Phys. Rev. D **77**, 094510 (2008).
[56] Marcela Pelaez, Matthieu Tissier, and Nicolas Wschebor, Three-point correlation functions in Yang-Mills theory, Phys. Rev. D **88**, 125003 (2013).
[57] Ph. Boucaud, M. Brinet, F. De Soto, V. Morenas, O. Pène, K. Petrov, and J. Rodríguez-Quintero, Three-gluon running coupling from lattice QCD at $N_f = 2 + 1 + 1$: A consistency check of the OPE approach, J. High Energy Phys. 04 (2014) 086.
[58] Adrian Blum, Markus Q. Huber, Mario Mitter, and Lorenz von Smekal, Gluonic three-point correlations in pure Landau gauge QCD, Phys. Rev. D **89**, 061703 (2014).
[59] Gernot Eichmann, Richard Williams, Reinhard Alkofer, and Milan Vujinovic, The three-gluon vertex in Landau gauge, Phys. Rev. D **89**, 105014 (2014).
[60] Mario Mitter, Jan M. Pawlowski, and Nils Strodthoff, Chiral symmetry breaking in continuum QCD, Phys. Rev. D **91**, 054035 (2015).
[61] Richard Williams, Christian S. Fischer, and Walter Heupel, Light mesons in QCD and unquenching effects from the 3PI effective action, Phys. Rev. D **93**, 034026 (2016).
[62] Adrian L. Blum, Reinhard Alkofer, Markus Q. Huber, and Andreas Windisch, Unquenching the three-gluon vertex: A status report, Acta Phys. Pol. B Proc. Suppl. **8**, 321 (2015).
[63] Anton K. Cyrol, Leonard Fister, Mario Mitter, Jan M. Pawlowski, and Nils Strodthoff, Landau gauge Yang-Mills correlation functions, Phys. Rev. D **94**, 054005 (2016).
[64] A. Athenodorou, D. Binosi, Ph. Boucaud, F. De Soto, J. Papavassiliou, J. Rodriguez-Quintero, and S. Zafeiropoulos, On the zero crossing of the three-gluon vertex, Phys. Lett. B **761**, 444 (2016).
[65] Ph. Boucaud, F. De Soto, J. Rodríguez-Quintero, and S. Zafeiropoulos, Refining the detection of the zero crossing for the three-gluon vertex in symmetric and asymmetric momentum subtraction schemes, Phys. Rev. D **95**, 114503 (2017).
[66] A. C. Aguilar, F. De Soto, M. N. Ferreira, J. Papavassiliou, and J. Rodríguez-Quintero, Infrared facets of the three-gluon vertex, Phys. Lett. B **818**, 136352 (2021).
[67] A. C. Aguilar, C. O. Ambrósio, F. De Soto, M. N. Ferreira, B. M. Oliveira, J. Papavassiliou, and J. Rodríguez-Quintero, Ghost dynamics in the soft gluon limit, Phys. Rev. D **104**, 054028 (2021).
[68] Anthony G. Duarte, Orlando Oliveira, and Paulo J. Silva, Further evidence for zero crossing on the three gluon vertex, Phys. Rev. D **94**, 074502 (2016).
[69] Lukas Corell, Anton K. Cyrol, Mario Mitter, Jan M. Pawlowski, and Nils Strodthoff, Correlation functions of three-dimensional Yang-Mills theory from the FRG, SciPost Phys. **5**, 066 (2018).
[70] A. C. Aguilar, F. De Soto, M. N. Ferreira, J. Papavassiliou, J. Rodríguez-Quintero, and S. Zafeiropoulos, Gluon propagator and three-gluon vertex with dynamical quarks, Eur. Phys. J. C **80**, 154 (2020).
[71] A. C. Aguilar, M. N. Ferreira, C. T. Figueiredo, and J. Papavassiliou, Gluon mass scale through nonlinearities and vertex interplay, Phys. Rev. D **100**, 094039 (2019).
[72] Nahuel Barrios, Marcela Peláez, and Urko Reinosa, Two-loop three-gluon vertex from the Curci-Ferrari model and its leading infrared behavior to all loop orders, Phys. Rev. D **106**, 114039 (2022).
[73] F. Pinto-Gómez, F. De Soto, M. N. Ferreira, J. Papavassiliou, and J. Rodríguez-Quintero, Lattice three-gluon vertex in extended kinematics: Planar degeneracy, Phys. Lett. B **838**, 137737 (2023).
[74] F. Pinto-Gómez, The three-gluon vertex from quenched lattice QCD in Landau gauge, Few-Body Syst. **64**, 43 (2023).
[75] Joseph Meyers and Eric S. Swanson, Spin zero glueballs in the Bethe-Salpeter formalism, Phys. Rev. D **87**, 036009 (2013).
[76] Daniele Binosi, Lei Chang, Joannis Papavassiliou, and Craig D. Roberts, Bridging a gap between continuum-QCD and *ab initio* predictions of hadron observables, Phys. Lett. B **742**, 183 (2015).

[77] Emanuel V Souza, Mauricio Narciso Ferreira, Arlene Cristina Aguilar, Joannis Papavassiliou, Craig D Roberts, and Shu-Sheng Xu, Pseudoscalar glueball mass: A window on three-gluon interactions, Eur. Phys. J. A **56**, 25 (2020).
[78] Daniele Binosi, Cedric Mezrag, Joannis Papavassiliou, Craig D. Roberts, and Jose Rodriguez-Quintero, Process-independent strong running coupling, Phys. Rev. D **96**, 054026 (2017).
[79] Craig D Roberts, Empirical consequences of emergent mass, Symmetry **12**, 1468 (2020).
[80] Markus Q. Huber, Nonperturbative properties of Yang–Mills theories, Phys. Rep. **879**, 1 (2020).
[81] Andreas Athenodorou and Michael Teper, The glueball spectrum of SU(3) gauge theory in $3+1$ dimensions, J. High Energy Phys. 11 (2020) 172.
[82] Andreas Athenodorou and Michael Teper, SU(N) gauge theories in $3+1$ dimensions: Glueball spectrum, string tensions and topology, J. High Energy Phys. 12 (2021) 082.
[83] Markus Q. Huber, Christian S. Fischer, and Helios Sanchis-Alepuz, Higher spin glueballs from functional methods, Eur. Phys. J. C **81**, 1083 (2021).
[84] James S. Ball and Ting-Wai Chiu, Analytic properties of the vertex function in gauge theories. 1, Phys. Rev. D **22**, 2542 (1980).
[85] Anna Hasenfratz and Peter Hasenfratz, The connection between the lambda parameters of lattice and continuum QCD, Phys. Lett. **93B**, 165 (1980).
[86] Ph. Boucaud, F. De Soto, K. Raya, J. Rodríguez-Quintero, and S. Zafeiropoulos, Discretization effects on renormalized gauge-field Green's functions, scale setting, and the gluon mass, Phys. Rev. D **98**, 114515 (2018).
[87] C. Parrinello, Exploratory study of the three gluon vertex on the lattice, Phys. Rev. D **50**, R4247 (1994).
[88] B. Alles, D. Henty, H. Panagopoulos, C. Parrinello, C. Pittori, and D. G. Richards, α_s from the nonperturbatively renormalised lattice three gluon vertex, Nucl. Phys. **B502**, 325 (1997).
[89] C. Parrinello, D. G. Richards, B. Alles, H. Panagopoulos, and C. Pittori, Status of alpha-s determinations from the nonperturbatively renormalized three gluon vertex, Nucl. Phys. B, Proc. Suppl. **63**, 245 (1998).
[90] Philippe Boucaud, J. P. Leroy, J. Micheli, O. Pene, and C. Roiesnel, Lattice calculation of alpha(s) in momentum scheme, J. High Energy Phys. 10 (1998) 017.
[91] Andreas Athenodorou, Philippe Boucaud, Feliciano de Soto, José Rodríguez-Quintero, and Savvas Zafeiropoulos, Instanton dominance over α_s at low momenta from lattice QCD simulations at $N_f = 0$, $N_f = 2+1$ and $N_f = 2+1+1$, EPJ Web Conf. **175**, 12011 (2018).
[92] A. Athenodorou, Ph. Boucaud, F. De Soto, J. Rodríguez-Quintero, and S. Zafeiropoulos, Instanton liquid properties from lattice QCD, J. High Energy Phys. 02 (2018) 140.
[93] Silvia Necco and Rainer Sommer, The $N_f = 0$ heavy quark potential from short to intermediate distances, Nucl. Phys. **B622**, 328 (2002).
[94] D. Becirevic, Ph. Boucaud, J. P. Leroy, J. Micheli, O. Pene, J. Rodriguez-Quintero, and C. Roiesnel, Asymptotic behaviour of the gluon propagator from lattice QCD, Phys. Rev. D **60**, 094509 (1999).
[95] D. Becirevic, Ph. Boucaud, J. P. Leroy, J. Micheli, O. Pene, J. Rodriguez-Quintero, and C. Roiesnel, Asymptotic scaling of the gluon propagator on the lattice, Phys. Rev. D **61**, 114508 (2000).
[96] F. de Soto, Restoring rotational invariance for lattice QCD propagators, J. High Energy Phys. 10 (2022) 069.
[97] F. de Soto and C. Roiesnel, On the reduction of hypercubic lattice artifacts, J. High Energy Phys. 09 (2007) 007.
[98] Philippe Boucaud, F. De Soto, J. P. Leroy, A. Le Yaouanc, J. Micheli *et al.*, Ghost-gluon running coupling, power corrections and the determination of $\Lambda_{\overline{\rm MS}}$, Phys. Rev. D **79**, 014508 (2009).
[99] B. Blossier, Ph. Boucaud, F. De soto, V. Morenas, M. Gravina, O. Pene, and J. Rodriguez-Quintero, Ghost-gluon coupling, power corrections and $\Lambda_{\overline{\rm MS}}$ from twisted-mass lattice QCD at $N_f = 2$, Phys. Rev. D **82**, 034510 (2010).
[100] B. Blossier, Ph. Boucaud, M. Brinet, F. De Soto, X. Du, V. Morenas, O. Pene, K. Petrov, and J. Rodriguez-Quintero, The strong running coupling at τ and Z_0 mass scales from lattice QCD, Phys. Rev. Lett. **108**, 262002 (2012).
[101] S. Zafeiropoulos, P. Boucaud, F. De Soto, J. Rodríguez-Quintero, and J. Segovia, Strong running coupling from the gauge sector of domain wall lattice QCD with physical quark masses, Phys. Rev. Lett. **122**, 162002 (2019).
[102] Zhu-Fang Cui, Jin-Li Zhang, Daniele Binosi, Feliciano de Soto, Cédric Mezrag, Joannis Papavassiliou, Craig D. Roberts, Jose Rodríguez-Quintero, Jorge Segovia, and Savvas Zafeiropoulos, Effective charge from lattice QCD, Chin. Phys. C **44**, 083102 (2020).
[103] A. Athenodorou, Ph. Boucaud, F. De Soto, J. Rodríguez-Quintero, and S. Zafeiropoulos, Gluon Green functions free of quantum fluctuations, Phys. Lett. B **760**, 354 (2016).
[104] M. Peláez, M. Tissier, and N. Wschebor, Two-point correlation functions of QCD in the Landau gauge, Phys. Rev. D **90**, 065031 (2014).
[105] A. C. Aguilar, M. N. Ferreira, C. T. Figueiredo, and J. Papavassiliou, Nonperturbative structure of the ghost-gluon kernel, Phys. Rev. D **99**, 034026 (2019).